Agenzia Nazionale per le Nuove Tecnologie,
l'Energia e lo Sviluppo Economico Sostenibile

Ministero dello Sviluppo Economico

RICERCA DI SISTEMA ELETTRICO

Modellazione del comportamento di elio in combustibili MOX ad alto burn-up ai fini dell'estensione degli strumenti di simulazione e di supporto alla progettazione delle barrette di combustibile per i reattori di generazione evolutiva ad acqua pressurizzata

Lelio Luzzi, Pietro Botazzoli, Giovanni Pastore

Report RdS/2011/359

MODELLAZIONE DEL COMPORTAMENTO DI ELIO IN COMBUSTIBILI MOX AD ALTO BURN-UP AI FINI DELL'ESTENSIONE DEGLI STRUMENTI DI SIMULAZIONE E DI SUPPORTO ALLA PROGETTAZIONE DELLE BARRETTE DI COMBUSTIBILE PER I REATTORI DI GENERAZIONE EVOLUTIVA AD ACQUA PRESSURIZZATA

Lelio Luzzi, Pietro Botazzoli, Giovanni Pastore (Politecnico di Milano)

Novembre 2011

Report Ricerca di Sistema Elettrico
Accordo di Programma Ministero dello Sviluppo Economico – ENEA
Area: Governo, gestione e sviluppo del sistema elettrico nazionale
Progetto: Fissione nucleare: metodi di analisi e verifica di progetti nucleari di generazione evolutiva ad acqua pressurizzata

Responsabile Progetto: Massimo Sepielli, ENEA

ENEA Ricerca Sistema Elettrico	Sigla di identificazione	Distrib.	Pag.	di
	PAR2010-CIRTEN-LB1-016	L	1	

Titolo

"Modellazione del comportamento di elio in combustibili MOX ad alto burn-up ai fini dell'estensione degli strumenti di simulazione e di supportoalla progettazione delle barrette di combustibile per i reattori di generazione evolutiva ad acqua pressurizzata".

Ente emittente CIRTEN

PAGINA DI GUARDIA

Descrittori

Tipologia del documento: **Rapporto tecnico**

Collocazione contrattuale: ACCORDO DI PROGRAMMA Ministero dello Sviluppo Economico – ENEA sulla Ricerca di Sistema Elettrico PIANO ANNUALE DI REALIZZAZIONE 2010 Progetto 1.3.2.a: Fissione nucleare: Metodi di analisi e verifica di progetti nucleari di generazione evolutiva ad acqua pressurizzata.

Argomenti trattati: Combustibile nucleare

Sommario

The object of the present report is the study and modelling of the behaviour of inert gases (with particular emphasis on helium) in oxide nuclear fuels (UO_2 and MOX) of Light Water Reactors (LWR). Numerical simulations by means of dedicated codes, and their assessment on the basis of experimental data, have been performed in order to better understand the mechanisms involved in the considered phenomena and to propose models suitable for the implementation in fuel performance codes. Although the proposed models have been implemented in the TRANSURANUS code, the studies carried out are of more general applicability.

Note

Lavoro eseguito da CIRTEN, Politecnico di Milano, Dip.to di Energia.
Obiettivo 1.2 Contratto ENEA-CIRTEN.

Copia n. **In carico a:**

REV.	DESCRIZIONE	DATA		CONVALIDA	VISTO	APPROVAZIONE
2			NOME			
			FIRMA			
1			NOME			
			FIRMA			
0	EMISSIONE		NOME			
			FIRMA	M. Ciotti	M.Sepielli	M. Sepielli

CIRTEN

Consorzio Interuniversitario per la Ricerca TEcnologica Nucleare

POLITECNICO DI MILANO

Dipartimento di Energia, Sezione Ingegneria Nucleare

CeSNEF – Centro Studi Nucleari Enrico Fermi

Modellazione del comportamento di elio in combustibili MOX ad alto burn-up ai fini dell'estensione degli strumenti di simulazione e di supporto alla progettazione delle barrette di combustibile per i reattori di generazione evolutiva ad acqua pressurizzata

Autori

Lelio Luzzi

Pietro Botazzoli

Giovanni Pastore

CERSE-POLIMI RL 1470/2011

MILANO, Novembre 2011

Lavoro svolto in esecuzione dell'Obiettivo 1.2 − Attività B.1: Studio dei combustibili ad alto burn-up
AdP MSE−ENEA sulla Ricerca di Sistema Elettrico - Piano Annuale di Realizzazione 2010
Progetto 1.3.2.a "Fissione nucleare: Metodi di analisi e verifica di progetti nucleari di generazione evolutiva alimentati ad acqua pressurizzata"

(This page has been intentionally left blank)

Contents

Executive summary

The study of the thermo-mechanical behaviour of fuel rods (fuel rod performance) is of paramount importance for the design, safety and licensing of nuclear fuels. In fact, the fuel rod is the first barrier against the release of fission products. The thermo-mechanical behaviour of the fuel rod is influenced by many phenomena coupling the fuel pellets and the cladding. The synergy of the different phenomena can be studied only by means of expensive and demanding integral irradiation tests, with the support of fuel performance codes. Many fuel performance codes have been developed in the last 40 years. Among them, TRANSURANUS, developed at the JRC-ITU (Joint Research Centre – Institute for Transuranium Elements, Karlsruhe, Germany) and available at Politecnico di Milano, is one of the most qualified tool. Although it is more than 30 years old, it is continuously under development in order to improve its prediction capabilities in view of increasing burn-ups and with the employment of new materials. For this end, the properties of new materials have to be implemented and semi-empirical correlations have to be replaced by more flexible physics-based models based on a multi-scale approach. The lifetime extension of a fuel rod at high burn-up, the fuel performance modelling in such conditions, and the improvement of the multi-scale approach applied to the behaviour of nuclear materials are important issues, which are supported by many International Projects (e.g., IFPE - International Fuel Performance Experiment, FUMEX-3 - FUel Modelling at EXtended burn-up, and F-BRIDGE - Basic Research for Innovative Fuel Design for GEN IV systems, sponsored by OECD/NEA, IAEA and the European Commission, respectively).

Among the issues currently investigated, the behaviour of inert gases in oxide fuels at high burn-up is one of the most relevant. In particular, the present work contributes to the study and the modelling of the He behaviour (from its production to the release) in oxide nuclear fuels for LWRs. Helium (He) behaviour can influence the in-reactor performance and the long term storage of nuclear fuel. During the irradiation, He trapped in the pellet can contribute to the degradation of the properties of the fuel. On the other hand, the fraction released in fuel rod free volume influences the inner pressure with consequences for the safety. This is especially relevant for Mixed OXide fuels (MOX), which are envisaged to be employed for a better sustainability of the nuclear energy resources (closed fuel cycle) and for the management of military grade plutonium (e.g., Fissile Material Disposition Program). In fact, He production increases exponentially with the burn-up and it is more relevant for MOX fuel, since the initial presence of Pu leads to a larger production of α emitters. To this end, in the present work, models relevant for the performance of LWR UO_2 and MOX fuels at high burn-ups have been developed, coupled and implemented in TRANSURANUS.

As a first step, a model for the production of He has been developed and implemented in the TRANSURANUS Burn-up module (TUBRNP). The model takes into account the He produced by α decays, (n,α) reactions and ternary fissions. At first, it has been verified through neutron-transport depletion calculations, performed by means of the VESTA Monte Carlo-depletion code (developed at the Institut de Radioprotection et Sûreté Nucléaire, France). Finally, the model has been validated against experimental data. In particular, a good agreement has been found in terms of average concentrations and radial profiles of the main α emitters produced in UO_2 fuels. However, further experimental data are needed for a more exhaustive validation of the model. The most important missing information is the He produced. Moreover, isotopic compositions and relative radial nuclide profiles of LWR MOX fuels, especially at high burn-up, are also relevant.

As a second step, the transport of He in the fuel has been investigated. A model for the He release in the rod free volume has been developed. In a simple but physics-based way, it takes into account the intra- and inter-granular behaviour and the absorption. The model has been implemented in TRANSURANUS

and preliminarily validated on the basis of pressurized and unpressurized fuel rods. The agreement is satisfactory, although some discrepancies have been noticed. More experimental data are needed for better assessing the model parameters (diffusion coefficient, solubility) and for a proper validation.

In summary, the behaviour of He in LWR fuel has been studied and modelled, considering the production, the release in the fuel rod free volume and the absorption. Some data would be useful for a more complete validation of the He production and release models of LWR MOX fuels. Although related to LWR conditions, the present work could be extended to fast reactors. This could be achieved by including specific one-group cross sections in the He production model, by considering the columnar grain growth and the corresponding release process from columnar grains.

List of figures

List of tables

(This page has been intentionally left blank)

List of acronyms

BNFL	British Nuclear Fuel Laboratory
BR	Branching Ratio
BWR	Boiling Water Reactor
EAF	European Activation File
EC	Electron Capture
ENDF	Evaluated Nuclear Data File
EPMA	Electron Probe Micro Analysis
FBR	Fast Breeder Reactor
F-BRIDGE	Basic Research for Innovative fuel Design for GEN IV systems
FG	Fission Gas
FGR	Fission Gas Release
FMDP	Fissile Material Disposition Program
FUMEX-3	FUel Modelling at EXtended burn-up
HM	Heavy Metal
HWR	Heavy Water Reactor
IAEA	International Atomic Energy Agency
IFPE	International Fuel Performance Experiment
JAERI	Japan Atomic Energy Research Institute

JANIS	JAva-based Nuclear Information Software
JEFF	Joint Evaluated Fission and Fusion file
JENDL	Japanese Evaluated Nuclear Data Library
JRC/ITU	Joint Research Centre/Institute for Transuranium Elements
LWR	Light Water Reactor
MFPR	Mechanism of FP Release code
MIMAS	MIcronized MASterblend
MOX	Mixed OXide fuels
O/M	Oxygen over Metal ratio
OECD/NEA	Organisation for Economic Co-operation and Development/Nuclear Energy Agency
ORIGEN	Oak Ridge Isotope GENeration
ORNL	Oak Ridge National Laboratory
PWR	Pressurized Water Reactor
SBR	Short Binderless Route
SCALE	Standardized Computer Analyses for Licensing Evaluation
SFCOMPO	Spent Fuel isotopic COMPOsition database
SIMS	Secondary Ion Mass Spectrometry
STP	Standard Temperature and Pressure
TF	Ternary Fission
TU	TRANSURANUS
TUBRNP	TransUranus BuRN-uP model

Introduction

The study of the thermo-mechanical behaviour of fuel rods (fuel rod performance) is of paramount importance for the design, safety analysis and licensing of nuclear fuels. In fact, the fuel rod is the first barrier against the release of fission products. In the standard configuration, it is composed by ceramic pellets in-piled in a metallic cladding. The thermal and mechanical behaviour of the fuel rod in reactor is influenced by many phenomena coupling the fuel pellets and the cladding (Olander, 1976). The synergy of the different phenomena can be studied only by means of expensive and demanding integral irradiation tests, with the support of fuel performance codes (Aybar and Ortego, 2005; Van Uffelen, 2006; Cacuci, 2010). A number of fuel performance codes have been developed in the last 40 years by several universities and research institutes. Among them, the TRANSURANUS (TU) code (Lassman, 1992), developed at the JRC/ITU (Joint Research Centre/Institute for Transuranium Elements, Karlsruhe, Germany), is one of the most qualified tool. Although developed more than 30 years ago, it is continuously under development in order to achieve reliable predictions in view of increasing fuel burn-up and employing innovative materials. For this end, the properties of new materials have to be implemented and semi-empirical correlations have to be replaced by more flexible physics-based models, developed on the basis of the results of different modelling techniques with different spatial and temporal scales (multi-scale approach), and supported by experiments. The lifetime extension of a fuel rod at high burn-up, the fuel performance modelling in such conditions, and the improvement of the multi-scale approach applied to the description of the behaviour of nuclear materials are important issues to be investigated. These issues are supported by many International Projects, such as IFPE (International Fuel Performance Experiment, http://www.nea.fr/science/fuel/ifpelst.html), FUMEX-3 (FUel Modelling at EXtended burn-up (Killeen et al., 2009), and F-BRIDGE (Basic Research for Innovative Fuel Design for GEN IV systems, http://www.f-bridge.eu/index.php/Technical-Description/), sponsored by OECD/NEA (Organisation for Economic Co-operation and Development/Nuclear Energy Agency), IAEA (International Atomic Energy Agency) and the European Commission, respectively.

Among the issues currently investigated, the production and the behaviour of inert gases in oxide fuels at high burn-up is one of the most important. This topic is especially relevant for the (U,Pu) Mixed OXide fuels (MOX), which are envisaged to be employed both for a better sustainability of the nuclear energy resources (closed fuel cycle) and for the management of military grade plutonium (e.g., FMDP - Fissile Material Disposition Program). In particular, helium production and behaviour is of relevance in view of increasing burn-ups and linear heat generation rates, since its production increases exponentially as a function of the burn-up. This can have two important consequences: (i) if trapped in the pellets, helium can contribute to the degradation of the fuel thermal conductivity and swelling; (ii) if helium diffuses to the gap between the fuel and the cladding, it enhances the rod pressure with important consequences for the safety.

The object of the present report is the study and modelling of the behaviour of inert gases (with particular emphasis on helium) in oxide nuclear fuels (UO_2 and MOX) of Light Water Reactors (LWR). Numerical simulations by means of dedicated codes, and their assessment on the basis of experimental data, have been performed in order to better understand the mechanisms involved in the considered phenomena and to propose models suitable for the implementation in fuel performance codes. Although the proposed models have been implemented in the TRANSURANUS code, the studies carried out are of more general applicability.

The report is structured in two chapters (further details of the work can be found in appendix).

In the first chapter, a model for the production of helium, developed in the context of the present work, is presented. The model has been implemented in the TransUranus BuRN-up module (TUBRNP) of the TRANSURANUS code. The neutron transport-depletion code VESTA has been used for the verification. Finally, experimental data available in the open literature and at JRC/ITU have been used for the validation.

In the second chapter, mechanisms for the release of helium during LWR operations are discussed. On the basis of the evaluated information, a model for the release of helium has been developed, coupled with the helium production and grain growth models in the TRANSURANUS code, and tested against experimental data.

Chapter 1
Helium production model

The evaluation of the helium produced in oxide nuclear fuel during both the operation and the shut-down periods is necessary for a quantitative description of its behaviour. In the present chapter, a model for the production of helium, which can be integrated in a fuel performance code, is presented. The model has been implemented in the TUBRNP module of the TRANSURANUS fuel performance code, verified by means of a detailed comparison with the VESTA neutron transport depletion code and validated against experimental data. An important feature of the model is the ability of predicting local helium production rates, which are influenced by the steep radial power profile, typical of LWR fuel rods. This feature is of relevance since the behaviour of helium is strongly affected by the temperature, which varies across the fuel pellet.

The chapter is structured as follows: in the first section, the mechanisms leading to the production of helium are discussed, a quick look at the available codes able to predict the production of helium is given, and the status of the TRANSURANUS fuel performance code before the present work is presented. In the second section, the model development and the parameter evaluation are discussed. In the third section, the model verification is presented by means of a comparison with the VESTA code and a sensitivity analysis is performed taking into account the uncertainty of the model parameters. In the last sections, the model validation is presented for the average concentrations and radial profiles.

1.1 Introduction

1.1.1 Helium production mechanisms

Helium is produced in reactor by means of: (i) α decays, (ii) (n,α) reactions and (iii) ternary fissions.

α decay contribution: the scheme of captures and decays, initiated by plutonium isotopes during the irradiation, is shown in Figure 1.1. Fission events should be added to all the nuclides but are not indicated for the sake of clarity. For the same reason, also the internal transition of ^{242m}Am to ^{242}Am is not shown. However, this contribution is negligible since it has a half life of 141 years. It is possible to notice that almost all the actinides are α emitters, but only ^{242}Cm, ^{243}Cm, ^{244}Cm and ^{238}Pu have a half life short enough to have a sufficient number of decays during the lifetime in reactor. Furthermore, ^{243}Cm is created only as a consequence of radiative captures on ^{242}Cm, which has a half life of 163 days, about 60 times shorter than that of ^{243}Cm. This means that the number of α emitted by ^{243}Cm is actually negligible compared to that of ^{242}Cm.

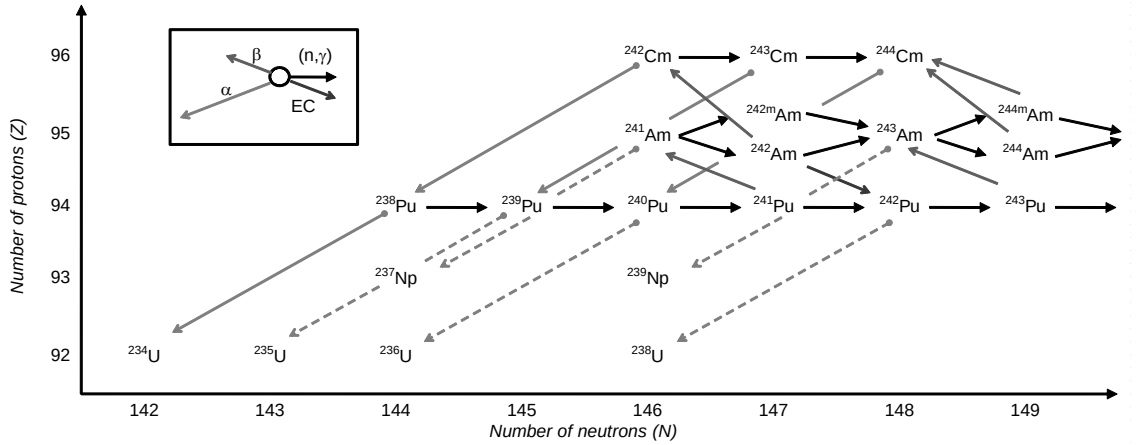

Figure 1.1 Scheme of captures and decays starting from the plutonium isotopes. β, α, and Electron Capture (EC) decays are indicated as well as radiative capture reactions (n,γ), while fissions (n, fiss) are not shown. Dashed lines are the decays with a half life larger than 100 years.

(n,α) reactions: the probability of occurrence of a nuclear reaction is commonly expressed in terms of an effective area (cross section - $\sigma(E)$) which is strongly dependent on the energy (E) of the incident particle. Figure 1.2a shows a comparison of the (n,α) cross sections of the most abundant isotopes in a nuclear fuel (^{16}O , ^{238}U, ^{235}U, and ^{239}Pu). The cross sections of ^{238}U, ^{235}U, and ^{239}Pu are very small and are in the range of few mbarn only for energies of the incident neutrons larger than 13-15 MeV,

which represent a negligible fraction (<0.1%) of the total amount of neutrons in the fuel of a LWR. On the contrary, the cross section of $^{16}O(n,\alpha)^{13}C$, which is a threshold reaction occurring only with neutrons with an energy larger than 2.36MeV, is in the order of tens/hundreds of mbarns for energies larger than 3.5-4 MeV. This represents some percent of the total amount of neutrons in the fuel of a LWR, meaning that the one-group effective cross sections - i.e., the cross sections averaged over the energy distribution (spectrum) of the neutrons - can be in the order of some mbarn. It is important to mention that, since negligible for fission reactors, the (n,α) cross sections of ^{238}U, ^{235}U, and ^{239}Pu are not present in the most used cross section libraries, i.e., the JEFF 3.1 (OECD/NEA, 2006), JENDL 4.0 (Shibata et al. 2010; Shibata et al., 2011), and ENDF B/VII.0 (Chadwick et al., 2006). The values in Figure 1.2 are taken from the European Activation File (EAF-2007), a neutron induced cross section library developed in the framework of the European Fusion programme (Forrest et al., 2007).

In Figure 1.2b, a comparison of the $^{16}O(n,\alpha)^{13}C$ of the JEFF 3.1, JENDL 4.0, and ENDF B/VII.0 libraries is shown. Large discrepancies exist between the different libraries. In fact, the cross section of the JEFF 3.1 is on average 35% larger than the JENDL 4.0 and ENDF B/VII.0 in the range of energies 2.36-9MeV, and the cross section of the JENDL 4.0 is 50% lower than the JEFF 3.1 and ENDF B/VII.0 in the range 10-20 MeV. However, the difference of the JENDL 4.0 is not important since only a negligible fraction of neutrons in the fuel of a LWR has energies larger than 10 MeV.

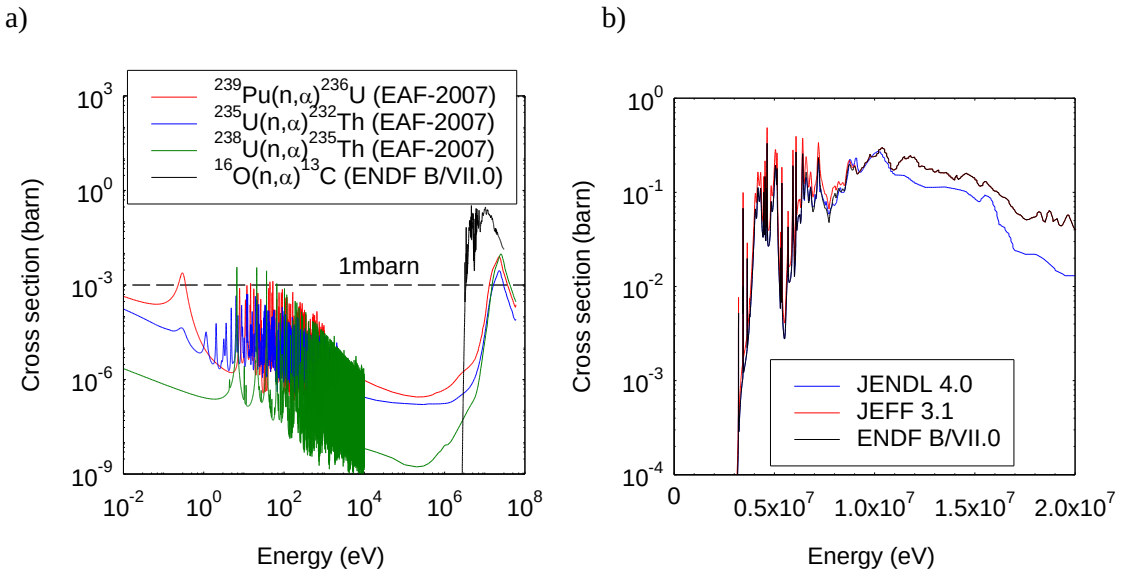

Figure 1.2 Comparison between a) the cross section of different (n,α) reactions and b) $^{16}O(n,\alpha)^{13}C$ cross sections from different libraries. Data have been taken from the Java-based Nuclear Information Software (JANIS), available online at http://www.oecd-nea.org/janis/.

Ternary fissions: during a fission event, two fission products and two/three neutrons are usually emitted. Additionally, a light atom (helium or, to a minor extent, hydrogen) is also emitted in 0.2÷0.3% of the cases (ternary fission). Figure 1.3 shows the probability of helium production (He yield) after a fission event. In particular, the values available in the JEFF 3.1 and JENDL 4.0 are compared for different fissile and fissionable isotopes. ENDF B/VII.0 library is not shown since it does not include ternary fission yields.

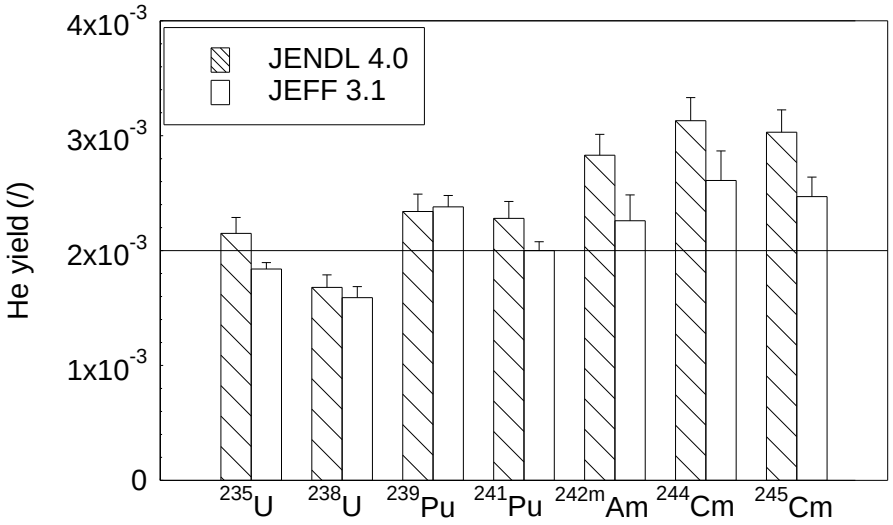

Figure 1.3 Comparison between the JEFF 3.1 and JENDL 4.0 yields of production of helium for different fissile and fissionable isotopes. The horizontal line represents an indicative value of 0.2%. Data have been taken from the Java-based Nuclear Information Software (JANIS).

1.1.2 Best estimate codes

The reference codes for estimating the amount of isotopes generated or depleted during the irradiation are called depletion codes. They simulate the build-up and the depletion of a large number of isotopes, taking into account decays and nuclear reactions.

The most widely used code is ORIGEN (Oak Ridge isotope generation and depletion code). Developed at Oak Ridge National Laboratories (ORNL) in the seventies, ORIGEN is available nowadays in different forms - e.g., ORIGEN2.2 (Croff, 1980), ORIGEN-ARP (Bowman et al., 1999), ORIGEN-JR (Bowman, 2007), ORIGEN-S (Bowman, 2007), ORIGEN-JUEL-II (Ruetten, 1993). It solves a system of non-homogeneous, first-order ordinary differential equation by means of the matrix exponential method, and using one-group effective cross sections available in built-in databases for different reactor spectra.

In order to have more reliable simulations, ORIGEN or other depletion codes are often coupled with neutron transport codes, able to compute spectra for a given geometrical configuration and isotopic composition. In this way, the specific geometry and the evolution of the isotopic compositions are taken into account at each time-step in the evaluation of the one-group effective cross sections. Among the huge variety of neutron transport-depletion codes, TRITON (Bowman, 2007) and VESTA (Haeck, 2009) are two examples. The former is a sub-module of the system SCALE (Standardized Computer Analyses for Licensing Evaluation - ORNL, 2006) which couples deterministic 2-D neutron transport calculations (by means of the NEWT sub-module) with ORIGEN-S calculations. The latter is conceived as a "generic" interface combining the ORIGEN 2.2 isotope depletion code with any version of Monte Carlo neutron transport codes, MCNP (Breismeister, 2000) or MCNPX (Pelowitz, 2005).

Since many of the isotopes evaluated by these codes are not relevant for the helium production, it would be not efficient coupling these kinds of codes with a fuel performance code. It is more efficient to include in a fuel performance code a simple model that takes into account only the isotopes relevant for the production of helium. However, neutron transport-depletion codes are a useful tool for the verification of simple models. In particular, in the present work, the VESTA code has been used for this purpose.

1.1.3 Status of the TRANSURANUS code before the present work

Helium production was already treated in the TRANSURANUS code. However, both the (n,α) and ternary fission contributions were not considered.

As concerns the α decay contribution, in its first version, it was considered in a simplified manner by coupling a numerical solution for the Pu isotopes (computed by the TRANSURANUS Burn-up module - TUBRNP, Lassmann et al., 1994) with a simple analytical solution for the Am and Cm nuclides. In particular, the decay and capture chains of Figure 1.1 were simplified in the two independent chains reported in Figure 1.4. This was made in order to fulfil the conditions for the existence of an analytical solution of the problem - i.e., (i) each of the nuclides occurs in the chain exactly once (“once-through” chain) and (ii) any source terms from further nuclides (outside the chain) can be neglected. In a later version of the model, the chains reported in Figure 1.4 have been included in TUBRNP, and extended by considering the missing neutron captures and decay. However, it is worth noting two simplifications of the chain A leading to an overestimation of ^{242}Cm still present in the last version of the model (before the present work). The first one concerns the (n,γ) reaction on ^{241}Am. In the chain A, this reaction leads always to ^{242}Am . However, this reaction should lead to ^{242m}Am with a branching ratio of 10-20% (as will be shown later). Since ^{242m}Am decays to ^{242}Am by internal conversion with a long half life (141 years), neglecting this branching ratio leads to an overestimation of ^{242}Am and then ^{242}Cm. The second

simplification concerns the decay of ^{242}Am. In the chain A, all the ^{242}Am decays β to ^{242}Cm. However, in 17.3% of the cases, this isotope should decay to ^{242}Pu by electron capture. It is important to mention that ^{242}Am is not modelled explicitly, but a fast decay is considered. Hence, all the captures on ^{241}Am lead to ^{242}Cm.

Another simplification concerning the chain B is that ^{244m}Am and ^{244}Am are not distinguished. This is a good approximation because both the metastable and ground states decay β with a short half life (26 minutes and 10 hours, respectively).

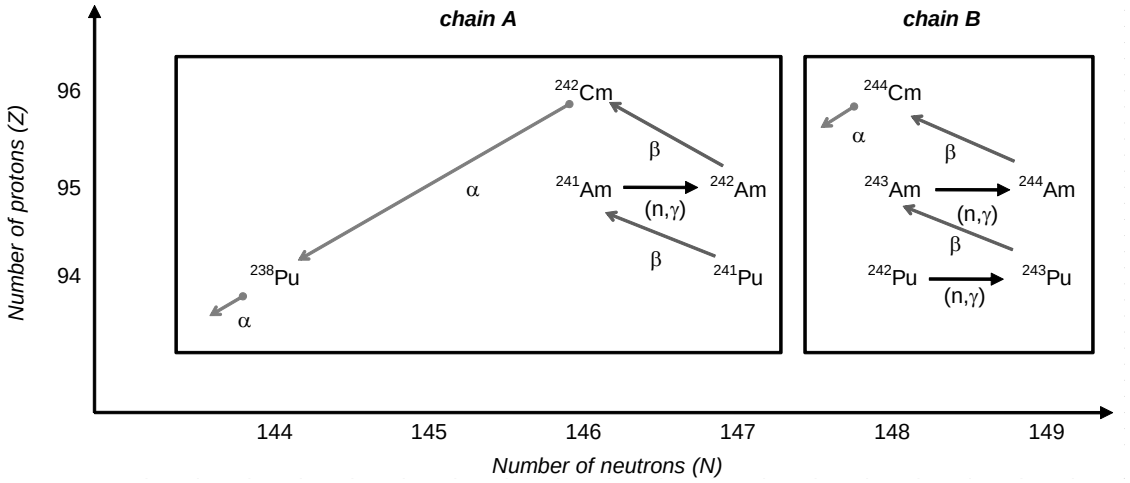

Figure 1.4 Simplified nuclide chains A and B used for the approximate calculation of the concentration of ^{4}He.

As written previously, plutonium isotopes are computed by TUBRNP, a sub-module of the TRANSURANUS code which calculates the radial power profile. In TUBRNP, the calculation is split into (a) the approximation of the neutron flux through thermal diffusion theory, and (b) the computation of the local concentrations of the isotopes influencing the radial power profile (i.e., ^{235,236,238}U, ^{237}Np, $^{238\text{-}242}$Pu, ^{241}Am, ^{243}Am, $^{242\text{-}245}$Cm) with simplified depletion equations:

$$dN_m(r) = \left[-\sigma_{a,m}N_m(r)f_m(r) + \sigma_{c,m-1}N_{m-1}(r)f_{m-1}(r)\right]\cdot A(r)\cdot dbu(r) + \left[-N_m(r)\lambda_m + \sum_i N_i(r)\lambda_i\right]\cdot dt \quad (1.1)$$

where r is the radial coordinate, $N_m(r)$ (at/cm^3) is the local concentration of the nuclide m, $\sigma_{a,m}$ (barn) and $\sigma_{c,m}$ (barn) are the one-group effective cross sections for total neutron absorption and neutron capture, respectively, $dbu(r)$ (MWd/kgHM) is the local burn-up increment referred to the initial Heavy Metal (HM) content, $A(r)$ is a conversion factor, λ_i (h^{-1}) the decay constant of the nuclide i, dt (h) the time-step and $f_m(r)$ is a form factor

that reflects the radial dependence of absorption of epi-thermal or resonance neutrons. Quasi-immediate β decay of ^{237}U, ^{238}Np, ^{239}U, ^{239}Np, ^{242}Am, ^{244}Am and ^{243}Pu are considered.

A(r) is computed by considering that *A(r)·dbu(r)* represents the increment of the total neutron fluence (*Φ·dt* – neutrons/barn) in the time step (*dt*) and that:

$$\frac{dn_{fiss}(r)}{dt} = \frac{q'''(r)}{E_{fiss}} = \rho_{HM} \cdot \frac{dbu(r)}{dt} \cdot \frac{1}{E_{fiss}} = \Phi(r) \cdot \sum_i N_i(r) \cdot \sigma_{fiss,i} \qquad (1.2)$$

where $n_{fiss}(r)$ (fissions/cm^3) is the density of fissions, $N_i(r)$ (at/cm^3) the concentration of the i-th nuclide, $\sigma_{fiss,i}$ (barn) the one-group fission cross section of the i-th nuclide, ρ_{HM} (kgHM/cm^3) the density of heavy metals and E_{fiss} (MWd) the energy released per fission.

By inverting equation (1.2), it is possible to find:

$$A(r) = \frac{\Phi(r) \cdot dt}{dbu(r)} = \frac{\rho_{HM}}{E_{fiss} \cdot \sum_i N_i(r) \cdot \sigma_{fiss,i}} \qquad (1.3)$$

The density of heavy metals should be a function of the radius. However, since it does not change considerably during the irradiation, a constant value is considered in TUBRNP. In particular, ρ_{HM} = 9.18·10^{-3} kgHM/cm^3 is obtained by considering the theoretical density of UO_2 (10.96·10^{-3} kg/cm^3) multiplied by one minus the fractional porosity (a typical value of 5% is assumed) and multiplied by the weight fraction of HM with respect to the weight of the oxide (238/(238+32) = 0.8815 kgHM/kg). Finally, an energy released per fission of 195 MeV is considered, leading to E_{fiss} = 3.6·10^{-22} MWd.

As far as the absorption of epi-thermal or resonance neutrons is concerned, the factor $f_m(r)$ is applied only to ^{238}U and ^{240}Pu and has the form:

$$f_m(r) = 1 + p_1 \exp\left(-p_2 \left(R_{fuel} - r\right)^{p3}\right) \qquad (1.4)$$

where R_{fuel} (cm) is the fuel outer radius, and p_1, p_2 and p_3 are empirical constants derived after comprehensive comparisons with measurements of fuel slices irradiated in LWRs (Lassmann et al., 1994) as well as in the Halden Heavy Water Reactor (HWR) (Lassmann et al., 1998). The function $N_m(r)·f_m(r)$ is normalized to the radially averaged concentration of the considered nuclide.

Different fission and capture one-group effective cross sections for different reactors and fuel enrichments are present in the dataset of TUBRNP, based on simulations with the depletion code SCALE (Schubert et al., 2008).

1.2 Model set-up

As discussed in the sub-section 1.1.1, the local helium build-up in a oxide fuel can be described by (i) the α decays of ^{242}Cm, ^{244}Cm and ^{238}Pu, (ii) (n,α) reaction on ^{16}O, and (iii) ternary fissions. These contributions can be modelled by the following ordinary differential equation:

$$\begin{aligned}\frac{dN_{He4}}{dt} = & + N_{Cm242}\cdot\lambda_{Cm242} + N_{Cm244}\cdot\lambda_{Cm244} + N_{Pu238}\cdot\lambda_{Pu238} \\ & + \sigma_{\alpha,O16}\cdot\Phi\cdot N_{O-16} \\ & + \frac{dn_{fiss}}{dt}\cdot y_{He}\end{aligned} \qquad (1.5)$$

where N (at/cm^3) are the atom concentrations, λ (h^{-1}) the decay constants, n_{fiss} (fissions/cm^3) the density of fissions, y_{He} the fission yield for the production of helium, $\sigma_{\alpha,O16}$ (barn) the one-group effective ^{16}O(n,α)^{13}C cross section, and Φ (neutrons/(barn·h)) the total neutron flux.

The first three terms represent the α decay contribution, the fourth term the (n,α) contribution, while the last is the ternary fission contribution.

1.2.1 α decay contribution

As far as the contribution due to the α decay of the actinides is concerned, ^{242}Cm, ^{244}Cm and ^{238}Pu concentrations and the corresponding decay constants have to be known. However, a correct evaluation of these concentrations requires a complete evaluation of the burn-up chains. For this purpose, the set of equations (1.1) available in TUBRNP have been reviewed and some simplifications have been removed. This is the case of the branching ratios for the ^{241}Am(n,γ) ^{242m}Am reaction and for the decay of ^{242}Am by electron capture, which (as already discussed) were not considered. However, some simplifications have been kept: (i) ^{242m}Am has not been included since its effect on the concentrations of ^{242}Am (by internal conversion decay) and ^{243}Am (by radiative capture) is negligible, (ii) as in the previously implemented helium production model, ^{244}Am has been considered as the sum of both the metastable and the ground states (they both decay β with a short half life, and (iii) the approximations of fast decays of ^{237}U, ^{238}Np, ^{239}U, ^{239}Np, ^{242}Am, ^{244}Am and ^{243}Pu already present in the TUBRNP model have been kept.

The model parameters to be evaluated were: (i) branching ratio for the decay of ^{242}Am by electron capture, and (ii) branching ratio for the ^{241}Am(n,γ) ^{242m}Am reaction. The former has been taken from the Karlsruher chart of nuclides, and a value of 17.3% has been implemented. The latter, depending on the energy of the incident neutron, has been evaluated as follows:

$$BR_{Am241(n,\gamma)Am242m} = \frac{\int_0^\infty \sigma_{Am241(n,\gamma)Am242m}(E)\cdot\Psi(E)dE}{\int_0^\infty \sigma_{Am241(n,\gamma)}(E)\cdot\Psi(E)dE} \qquad (1.6)$$

where E (eV) is the energy of the incident neutron, $\sigma_{Am241(n,\gamma)Am242m}(E)$ (barn) is the cross section for the reaction ^{241}Am(n,γ)^{242m}Am, $\sigma_{Am241(n,\gamma)}(E)$ (barn) is the cross section for the reaction (n,γ) on ^{241}Am, independent of the product, and $\Psi(E)$ (eV^{-1}) the neutron spectrum. The cross sections of the JENDL 4.0, JEFF 3.1 and ENDF B/VII.0 have been considered, while the neutron spectra have been evaluated by means of MCNP (Monte Carlo N-Particle) simulations, carried out for different fuel compositions in Pressurized Water Reactors (PWR) and Boiling Water Reactors (BWR) using the JEFF 3.1 libraries. As far as the BWR is concerned, since the water density should be a function of the fuel rod height, simulations with different densities (in the range 200, 800 kg/m^3) have been performed. More details about the MCNP modelling are given in Appendix A.

Figure 1.5 shows the results for different fuel compositions and cross section libraries a) for the PWR and b) for the BWR (considering different water densities). It is possible to see that the effective branching ratio is a function of the fuel enrichment, plutonium content and, in the case of BWR, of the water density. However, the adopted library has a larger influence. For this reason, a value of 12% has been considered for the implementation in the TRANSURANUS code, independent of the reactor and of the fuel composition.

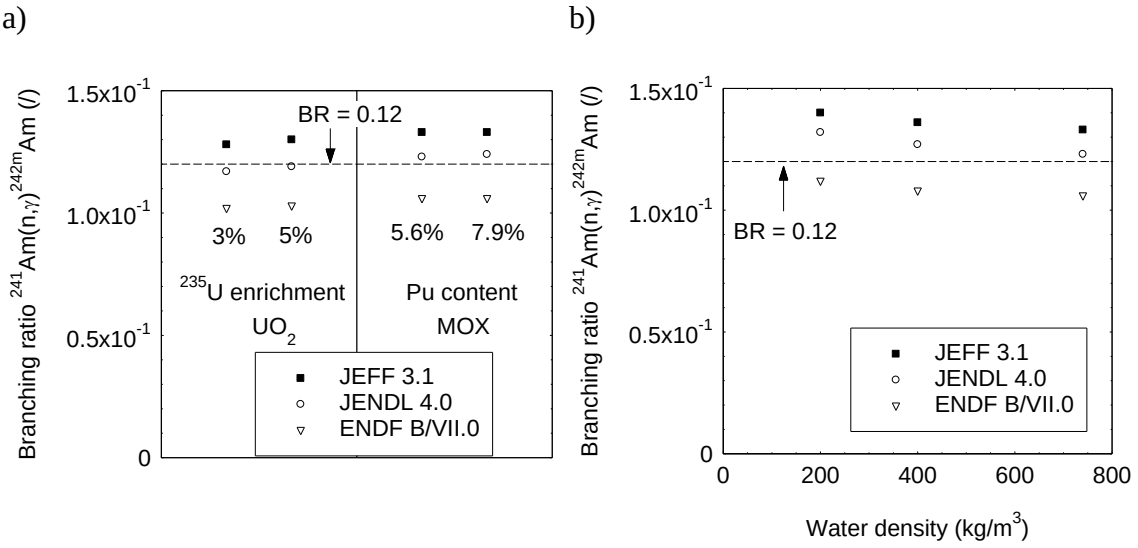

Figure 1.5 ^{241}Am(n,γ)^{242m}Am effective branching ratio computed with different cross section libraries: a) as a function of the enrichment and Pu content in PWR conditions and b) as a function of the water density for a MOX fuel with a Pu content of 5.6% in BWR conditions.

1.2.2 (n,α) contribution

As far as the (n,α) contribution is concerned, the one-group effective cross section of the reaction $^{16}O(n,\alpha)^{13}C$ and the concentration of ^{16}O as a function of time have to be known.

A complete study has been carried out for the $^{16}O(n,\alpha)^{13}C$ reaction adopting the cross sections of both the JEFF 3.1 and ENDF/B VII.0 libraries (JENDL 4.0 has not been considered since very similar to ENDF/B VII.0).

In Figure 1.6, the effective cross sections evaluated for different MOX configurations are shown. Although the $^{16}O(n,\alpha)^{13}C$ cross section of ENDF/B VII.0 has been considered the most reliable (Federici et al., 2007), the JEFF 3.1 cross section is shown for the PWR case for the purpose of comparison, highlighting an overestimation of about 40%. Two moderator densities are considered for the BWR case (400 and 600 kg/m^3) representing the range of the average density of a BWR channel. By comparing the PWR and BWR cross sections, the latter are 5 to 15% smaller, depending on the adopted average moderator density. Furthermore, a trend can be seen as a function of the plutonium content. However, because of the high uncertainty related to the cross section library, and because a different geometry can lead to a difference of a few percent, an average value of $3.2 \cdot 10^{-3}$ barn for PWR MOX fuel and an average value of $2.75 \cdot 10^{-3}$ barn for BWR MOX fuel have been included in the model.

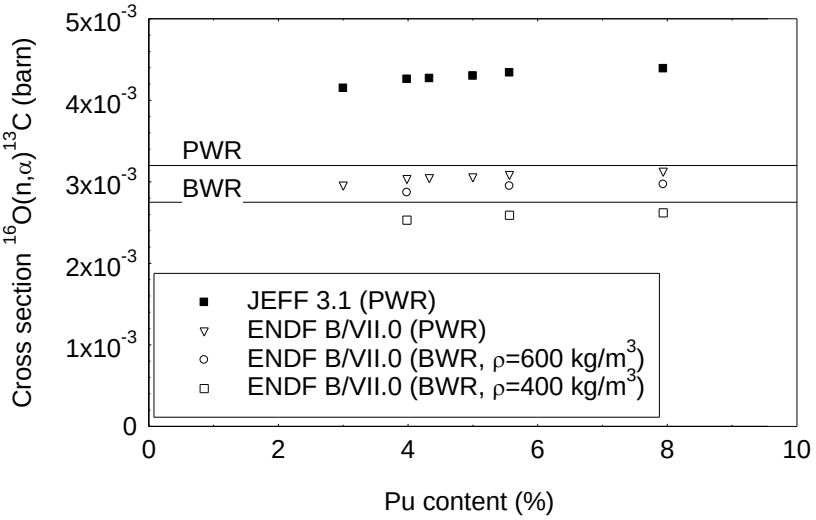

Figure 1.6 $^{16}O(n,\alpha)^{13}C$ cross section for different MOX fuels with different plutonium contents for both PWR and BWR conditions.

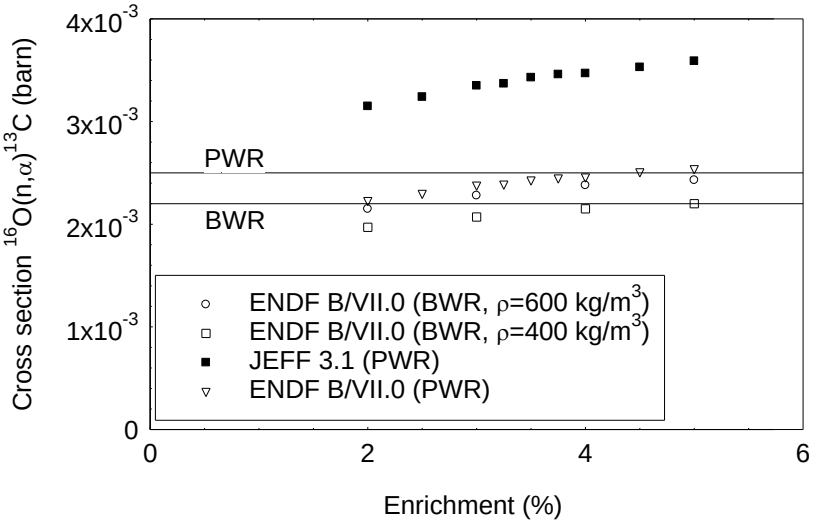

Figure 1.7 $^{16}O(n,\alpha)^{13}C$ cross section for UO_2 fuels with different enrichments for both PWR and BWR conditions.

Similar conclusions can be drawn from Figure 1.7, where the effective cross sections evaluated for PWR and BWR UO_2 fuels with different enrichments are shown. A value of $2.5 \cdot 10^{-3}$ barn for PWR UO_2 fuel and an average value of $2.2 \cdot 10^{-3}$ barn for BWR UO_2 fuel have been included in the model.

A second issue related to the $^{16}O(n,\alpha)^{13}C$ contribution concerns the concentration of ^{16}O as a function of time, which should be considered for the solution of Equation (1.5). However, this is expected to be very low, and then has not been included in the model. In order to confirm the degree of accuracy of this assumption, the following set of ordinary differential equations has been solved:

$$\begin{cases} \dfrac{dN_{O-16}}{dt} = -\sigma_{a,O16} \cdot N_{O16} \cdot \Phi \\ \dfrac{dN_{He-4}}{dt} = \sigma_{\alpha,O16} \cdot N_{O16} \cdot \Phi \end{cases} \tag{1.7}$$

where $\sigma_{a,O16}$ (barn) is the ^{16}O one-group total absorption effective cross section, $\sigma_{\alpha,O\text{-}16}$ (barn) the one-group effective $^{16}O(n,\alpha)^{13}C$ cross section, and Φ (neutrons/(barn·h)) the total neutron flux. It is important to mention that (n,α) reaction is the most probable, meaning that the one-group effective total absorption cross section is just slightly higher than the $^{16}O(n,\alpha)^{13}C$ cross section.

Assuming constant neutron flux and constant cross sections, the set of equations (1.7) can be analytically solved:

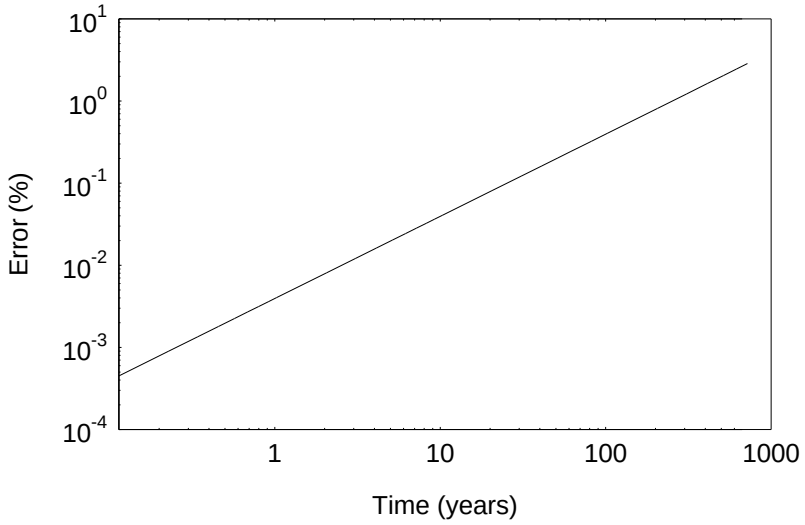

Figure 1.8 Error of the predicted helium (only (n,α) contribution) by means approximate solution (neglecting the oxygen consumption) with respect to the exact solution (equation (1.8)) as a function of time under constant conditions.

$$N_{He4}(t) = N_{O-16}(0) \cdot \frac{\sigma_{\alpha,O16}}{\sigma_{a,O16}} \cdot \left(1 - \exp\left(-\sigma_{a,O16} \cdot \Phi \cdot t\right)\right) \qquad (1.8)$$

For estimating the impact of using a constant oxygen concentration, a conservative value of $5 \cdot 10^{-3}$ barns ($=5 \cdot 10^{-27}$ cm^2) for both cross sections and a constant flux of $5 \cdot 10^{14}$ neutrons/(cm^{2}s) have been implemented in equation (1.8). In Figure 1.8**,** the error between the solution obtained neglecting the oxygen consumption and that one expressed by equation (1.8) is shown as a function of time. For the time scale of interest (less than 10 years), the discrepancy between the two approaches is negligible.

1.2.3 Ternary fission contribution

The ternary fission contribution is the number of fissions per unit of time and volume multiplied by the probability of production of helium after a fission event.

The number of fissions per unit of time and volume (fissions/cm^{3}h) is modelled by dividing the power density q''' (W/cm^3) by the energy released per fission (195 MeV = $8.68 \cdot 10^{-21}$Wh), in accordance with the treatment of other fission products (Cs, Xe, Kr) by means of TRANSURANUS.

A value of 0.22% proposed in (Federici et al., 2007) has been applied for the helium yield. A precise modelling of fission yields should consider the fissile isotope concentrations. Nevertheless, a constant value has been applied because (i) the values for different fissile isotopes, different incident neutron energies and different libraries are all in the range 0.15÷0.3 % (see sub-section 1.1.1), (ii) the values reported by

different libraries for the same nuclide can be quite different (see sub-section 1.1.1), and (iii) although not negligible, this contribution has a low influence on the total amount of helium produced (as will be shown in sub-section 1.3.3).

1.3 Model verification

The Monte Carlo depletion code VESTA has been used for the verification of the helium production model. Typical PWR conditions (geometry and materials) have been considered for the VESTA code simulations and two fuel compositions have been selected: UO_2 with an initial enrichment of 3.5%, and MOX with an initial Pu content of 5.6%. In Figure 1.9, the simulated power history is shown, reaching a burn-up of about 100 MWd/kgHM. For both initial compositions, four simulations have been run with different libraries, namely: (i) JEFF 3.1 cross section library plus the ORIGEN 2.2 fission yield database (case 1); (ii) JEFF 3.1 for both the cross sections and the fission yields (case 2); (iii) ENDF/B VII.0 cross section library plus the ORIGEN 2.2 fission yield database (case 3); and (iv) ENDF/B VII.0 for both the cross sections and the fission yields (case 4). It is important to mention that VESTA does not evaluate effective branching ratios from the cross section libraries, but it takes the values of the ORIGEN 2.2 dataset. In particular, the branching ratio for the $^{241}Am(n,\gamma)\ ^{242m}Am$ reaction of ORIGEN 2.2 is 20%, which is almost the double of the estimations of sub-section 1.2.1.

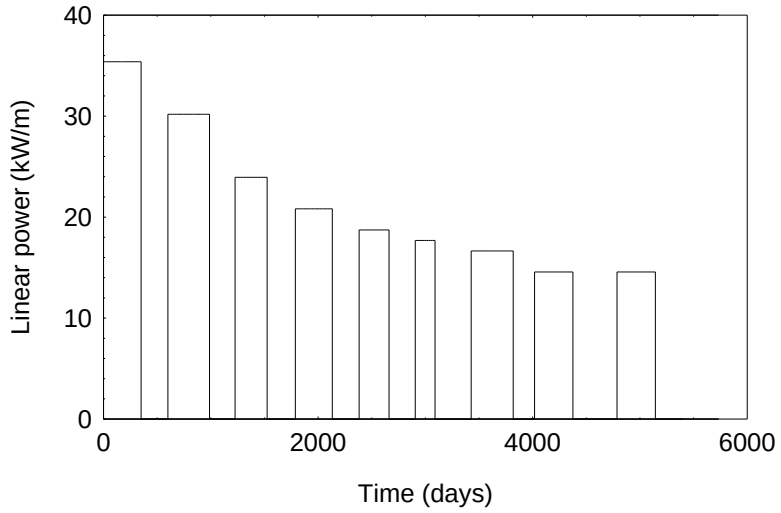

Figure 1.9 Simulated power history.

The quantities of interest computed by VESTA are:

- neutron flux as a function of time;
- concentrations of the main isotopes as a function of time;
- one-group cross sections of the most relevant reactions as a function of time.

These quantities have been compared with the results obtained by means of the TRANSURANUS code.

1.3.1 Total neutron flux

As a first step of the verification process, the formula implemented in TUBRNP for the computation of the total neutron flux (see equation (1.3)) has been independently evaluated considering the fission cross sections and the isotope concentrations computed by VESTA. The results are shown in Figure 1.10 for the MOX case 1. This graph is qualitatively representative of all simulated cases. The full line represents the neutron flux computed by the VESTA code, while the squares are the results obtained using the TRANSURANUS formula: an overestimation can be seen that increases as a function of time. The increasing overestimation can be explained by the fact that the TRANSURANUS formula considers only the main fissile and fissionable isotopes (i.e., ^{235}U, ^{238}U, ^{239}Pu, ^{240}Pu, ^{241}Pu and ^{242}Pu).

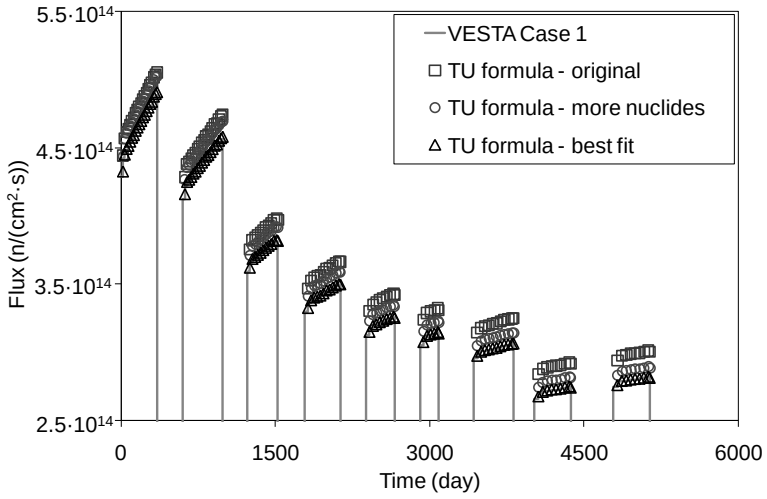

Figure 1.10 Comparison between the flux computed by VESTA and the results obtained by means of the TRANSURANUS (TU) formula.

At high burn-up important nuclides undergoing fissions are ^{245}Cm and ^{242m}Am due to their high fission cross sections. This can be seen in Figure 1.11, where the relative importance of the different nuclides on the total amount of fission (i.e. - fission cross section multiplied by the concentration normalized by the sum over all the nuclides) is shown. By including more nuclides in the denominator of equation (1.3) this overestimation disappears (circles). In order to explain the remaining overestimation, the real density of the fuel (11 g/cm^3 in the case of the MOX under consideration) has been considered and the energy released per fission has been modified in order to fit the VESTA results (triangles) achieving a value of about 210 MeV. Nevertheless, an error of 6-7% in the flux computation is acceptable considering the uncertainties related to the implemented one-group cross sections.

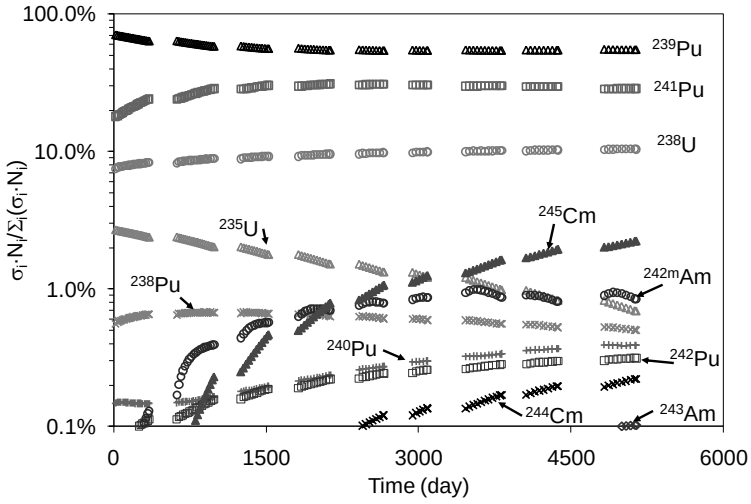

Figure 1.11 Weight of the different nuclides in the total number of fissions (VESTA case 1).

1.3.2 Verification of the burn-up chains

As a second step, in order to check the TRANSURANUS burn-up chains, the case-specific fission and capture cross sections computed by VESTA have been fitted as a function of the burn-up and implemented in a test version of the TRANSURANUS code (referred to as *TU best fit* in the graphs). Furthermore, the flux computation that fitted better to the VESTA results (triangles in Figure 1.10 – excluding ^{242m}Am) has been implemented in this version of the code. The comparison of the main isotope concentrations computed by VESTA and the results obtained by means of TRANSURANUS is satisfactory for all the cases. In Figure 1.12 and Figure 1.13, a comparison of the plutonium and curium concentrations is shown for the MOX case 1. The results obtained neglecting the branching ratios for the ^{241}Am(n,γ)^{242m}Am reaction and for the ^{242}Am decay by electron capture are also shown (*TU best fit, without BR*). In the case *TU best fit*, a value of 20% for the branching ratio for the ^{241}Am(n,γ)^{242m}Am

reaction has been considered in accordance to the ORIGEN 2.2 database. A good agreement can be noticed when the branching ratios (BR) are considered, while neglecting them leads to an overestimation of ^{242}Cm, ^{238}Pu and to a slight underestimation of ^{242}Pu. This can be explained by the fact that if we include the branching ratio for the reaction ^{241}Am(n,γ)^{242m}Am, less ^{242}Am is produced. Since ^{242}Am β decays to ^{242}Cm, less ^{242}Cm is produced, as well as ^{238}Pu (that results from the α decay of ^{242}Cm - as can be seen in Figure 1.1). Concerning the branching ratio for the ^{242}Am decay by electron capture (leading to ^{242}Pu), this path further decreases the production of ^{242}Cm and enhances the ^{242}Pu build-up. If ^{242}Cm, ^{244}Cm and ^{238}Pu are not well predicted, helium production cannot be correctly evaluated – see equation (1.5). The same conclusions can be drawn also for the other cases.

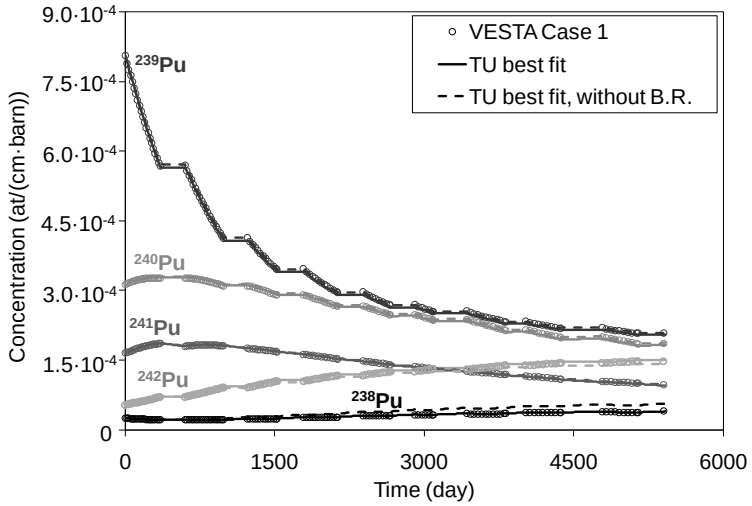

Figure 1.12 Plutonium concentrations: comparison between the predictions of VESTA, TU best fit and TU best fit without the branching ratios – Case 1 (JEFF 3.1 + ORIGEN), MOX.

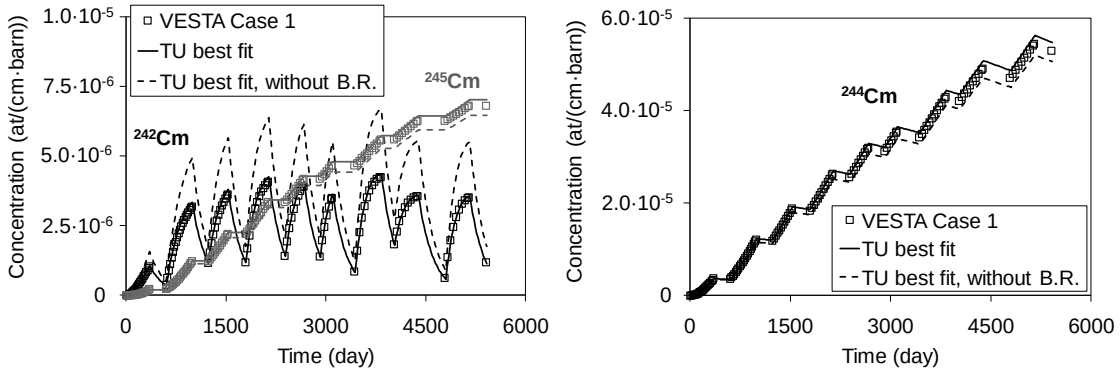

Figure 1.13 Curium concentrations: comparison between the predictions of VESTA, TU best fit and TU best fit without the branching ratios – Case 1 (JEFF 3.1 + ORIGEN), MOX.

In Figure 1.14 and Figure 1.15, the plutonium and curium concentrations computed by the TRANSURANUS version *TU best fit* are compared with the VESTA prediction for the UO_2 Case 4 (ENDF/B VII.0). A good agreement is noticed.

Figure 1.16 shows the comparison of produced helium for the MOX case 1 (JEFF 3.1+ORIGEN) and UO_2 cases 2 (JEFF 3.1) and 4 (ENDF/B VII.0). Case 3 is very similar to case 4 and therefore not shown. The symbols mark the VESTA results, while the TRANSURANUS results are indicated by lines.

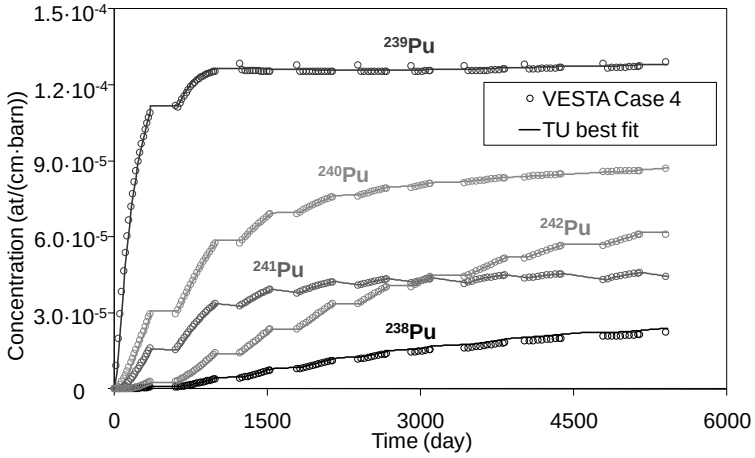

Figure 1.14 Plutonium concentrations: comparison between the predictions of VESTA and TU best fit – Case 4 (ENDF/B VII.0), UO_2.

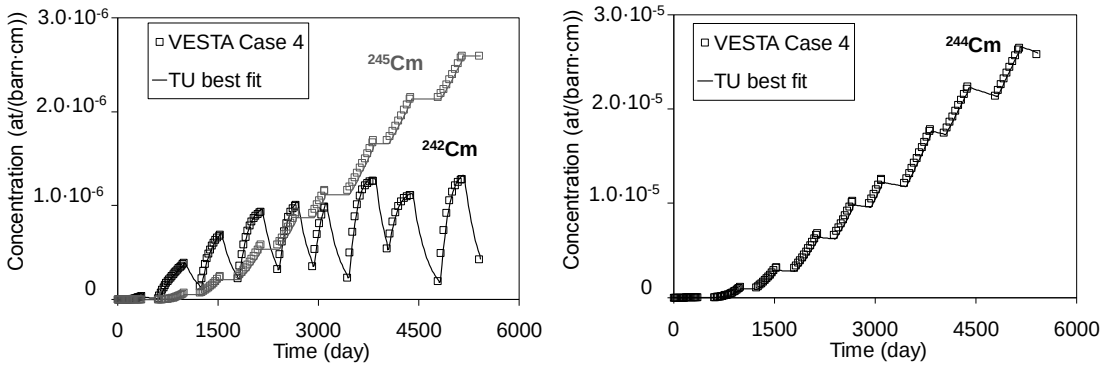

Figure 1.15 Curium concentrations: comparison between the predictions of VESTA and TU best fit – Case 4 (ENDF/B VII.0), UO_2.

Concerning the MOX case 1 and the UO_2 case 4, good agreement can be found when neglecting the ternary fission (TF), while for the UO_2 case 2 the agreement is good if the ternary fission contribution is considered. This is explained by the fact that the ORIGEN 2.2 fission yield database and the ENDF/B VII.0 library do not include the ternary fission yield, which is taken into account by JEFF 3.1. Furthermore, the effect of the branching ratios is shown for the MOX case: an overestimation occurs when they are neglected, due to the already explained overestimation of ^{242}Cm and ^{238}Pu. This overestimation is more significant for MOX, where the α-decay contribution is more important (due to the initial content of plutonium that produces more curium isotopes by neutron capture).

Two conclusions can be drawn:

- The set of equations implemented in the TRANSURANUS code correctly predicts the isotope concentrations, hence the considered isotopes are sufficient.
- When considering neutron transport codes: (i) the adopted cross section libraries play a fundamental role, as can be clearly noticed from the UO_2 cases 2 and 4 shown in Figure 1.16; (ii) fission yield databases do not always include the ternary fission yields (in these cases, the helium production is under-predicted).

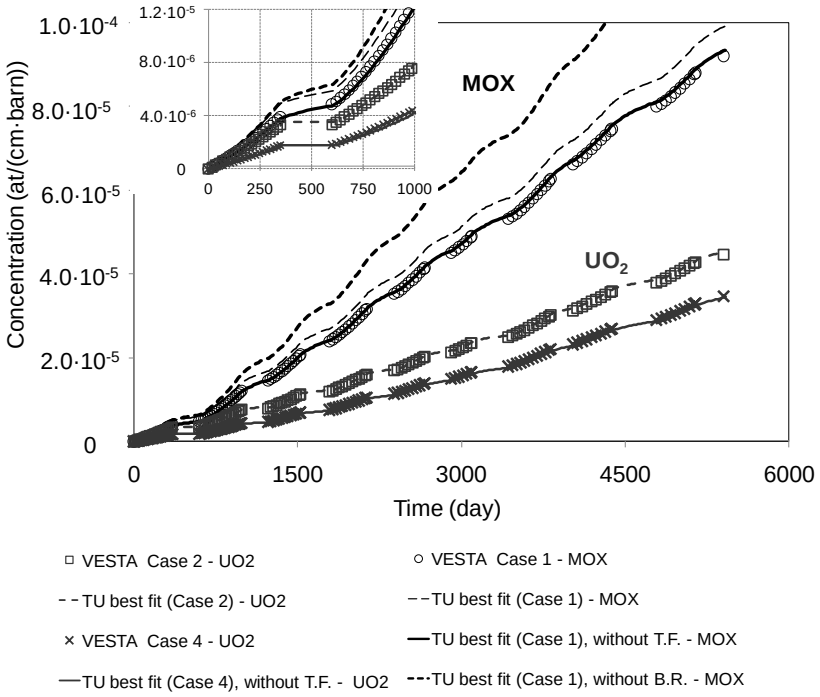

Figure 1.16 Helium production computed by TRANSURANUS (TU best fit version) and by VESTA. Grey symbols and lines correspond to the UO_2 cases, while black symbols and lines correspond to the MOX simulations.

1.3.3 Sensitivity analysis

As a further step for the assessment of the helium production model, a sensitivity analysis has been performed for the considered MOX fuel by means of the Taguchi method (for further details about the method, see Taguchi, 1987). In particular, the influence of four different input parameters on the calculated production of helium has been analysed: (i) the neutron flux; (ii) the $^{16}O(n,\alpha)^{13}C$ cross section; (iii) the ternary fission yield; and (iv) the capture and fission cross sections from different libraries.

In addition, the influence of the effect of the branching ratios for the $^{241}Am(n,\gamma)^{242m}Am$ reaction and for the decay of ^{242}Am by electron capture on the production of helium has been independently evaluated.

For evaluating the impact of the input parameters, the Taguchi method uses a special set of orthogonal arrays. These arrays stipulate the way of conducting the minimal number of simulations, which could give the full information of all the factors affecting the output parameter (in our case the helium produced). In particular, three representative values (levels) have been adopted for the four selected input parameters. In Table 1.1, the orthogonal array applied for the present case is shown. Nine simulations have been performed instead of 3^4 (=81) that would be necessary for a full factorial method. The three levels have been assigned as follows:

For the neutron flux, the original TRANSURANUS formula (level 1 – squares in Figure 1.10), the formula including more nuclides (level 2 –circles in Figure 1.10) and the "TU formula - best-fit" (level 3 – triangles in Figure 1.10, excluding ^{242m}Am) have been considered.

Table 1.1 Simulations setting in accordance with the Taguchi method.

Run	Levels			
	Flux model	$\sigma_{\alpha,O\text{-}16}$	Ternary fission yield	Cross sections library/dataset
1	1	1	1	1
2	1	2	2	2
3	1	3	3	3
4	2	1	2	3
5	2	2	3	1
6	2	3	1	2
7	3	1	3	2
8	3	2	1	3
9	3	3	2	1

For the $^{16}O(n,\alpha)^{13}C$ cross section, values of $3\cdot10^{-3}$ (level 1), $4\cdot10^{-3}$ (level 2) and $4.5\cdot10^{-3}$ (level 3) barn have been tested. Level 1 and level 3 correspond to the minimum and the maximum values found by means of MCNP with different MOX compositions and cross section libraries (see Figure 1.6).

For the ternary fission yield, the values of 0.18%, 0.2% and 0.22% have been chosen as level 1, 2 and 3, respectively.

Finally, for the capture and fission cross sections required by TRANSURANUS, the following levels have been set: the cross sections obtained with the VESTA cases 2 and 4 have been averaged as a function of the burn-up and implemented in TRANSURANUS (they correspond to the level 3 and 1, respectively), while the original dataset of TRANSURANUS has been used as level 2.

Figure 1.17 shows the influence that the different parameters have on the helium production at a burn-up of 60 MWd/kgHM (grey lines) and at the end of the simulated power history (about 100 MWd/kgHM – black lines). Results are normalized to the average value of the nine simulations. It is possible to notice that the most relevant parameter is the $^{16}O(n,\alpha)^{13}C$ cross section: it has an influence of about ±5% at 60 MWd/kgHM. It is slightly lower at the end of the irradiation when the contribution from the α decay is important (it increases exponentially as a function of the burn-up). The cross section library gives an uncertainty of about ±2÷3%: it increases as a function of the burn-up because the importance of the α decay contribution increases with burn-up. The choices of the flux model and of the ternary fission yield influence the helium production by about ±1%.

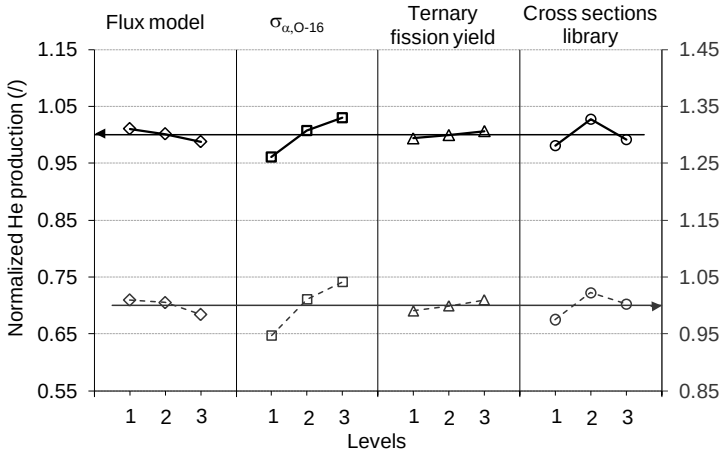

Figure 1.17 Influence of the parameters on the Helium produced at 60 MWd/kgHM (grey dashed lines and right axis) and at the end of life (black full lines and left axis).

The influence of the different parameters on the helium production at burn-up of 5 and 10 MWd/kgHM (Figure 1.18) has also been analysed, finding that the most influencing parameters are the $^{16}O(n,\alpha)^{13}C$ cross section and the ternary fission yield (they have an influence of ±10÷12% and about ±3%, respectively), whereas the choices of the flux model and of the cross section library influence the helium production by about ±1%. At such low burn-up, the contribution due to the α decay is negligible, hence the flux model and the cross section libraries have no influence, and the effects of the $^{16}O(n,\alpha)^{13}C$ cross section and of the ternary fission yield dominate.

The most important conclusions of the analysis by means of the Taguchi method are: (i) the cross section dataset and the TRANSURANUS formula for the flux computation already implemented in the code are sufficient to describe the helium production, the discrepancy at the end of life (at a very high burn-up of 100 MWd/kgHM) is of minor importance; (ii) a ternary fission yield of 0.22% independent of the fuel composition can be used because its influence on the total helium is low (a maximum of ±3%, when the burn-up is low and hence the production of helium is negligible); (iii) the $^{16}O(n,\alpha)^{13}C$ cross section is the most influencing parameter, and the value arising from the ENDF/B VII.0 library has to be considered the most reliable, based on the most recent measurements.

The effect of (i) the branching ratios for the $^{241}Am(n,\gamma)^{242m}Am$ reaction, and (ii) the ^{242}Am decay to ^{242}Pu due to electron capture on the helium production is shown in Figure 1.19. Neglecting the branching ratios leads to an overestimation of ^{242}Cm and ^{238}Pu, meaning an overestimation of produced helium by α-decay. This figure also shows that both branching ratios have quantitatively the same importance. Furthermore, comparing the results adopting a branching ratio for the $^{241}Am(n,\gamma)^{242m}Am$ reaction of 20% (i.e., the value adopted by ORIGEN) or 10% (lower value obtain in the analysis reported in section 1.2.1) a difference can be seen but this can be considered of second order in view of all the uncertainties of all the other parameters.

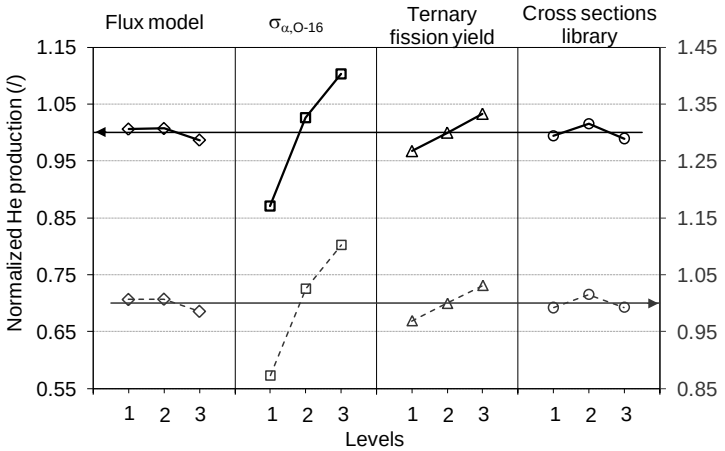

Figure 1.18 Influence of the parameters on the helium produced at 10 MWd/kgHM (grey lines and right axis) and at 5 MWd/kgHM (black lines and left axis).

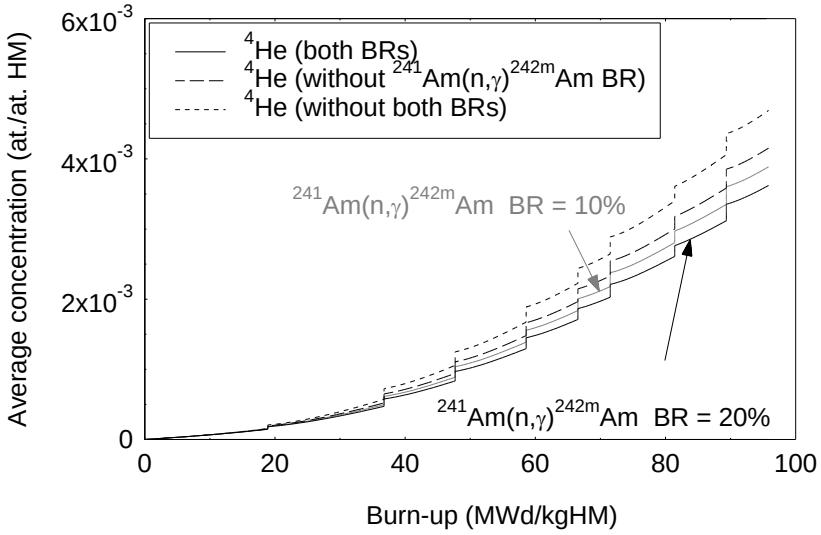

Figure 1.19 Helium production as a function of the burn-up for the MOX case computed by means of the TUBRNP model. The influence of the branching ratios (BR) for the $^{241}Am(n,\gamma)^{242m}Am$ reaction and for the ^{242}Am decay to ^{242}Pu due to electron capture is shown.

1.3.4 Helium production: comparison between TRANSURANUS and VESTA results

The MOX and UO_2 cases have been simulated by means of the updated version of the code and the results in terms of helium production are shown in Figure 1.20 (up to 30 MWd/kgHM) and Figure 1.21 (complete simulation up to 100 MWd/kgHM).

All results lie between the two extreme cases computed by VESTA (cases 2 and 3), and are closer to the case 2. This is in accordance with the fact that: (i) the $^{16}O(n,\alpha)^{13}C$ cross section implemented in TRANSURANUS has been evaluated on the basis of the ENDF/B VII.0 library (the same used for the case 3), which is about 40% lower than that one of JEFF 3.1 (used in the case 2), and the branching ratio for the $^{241}Am(n,\gamma)^{242m}Am$ reaction of TRANSURANUS is almost half of the value used by VESTA (12 against 20%), leading to a larger prediction of ^{242}Cm and then of helium by α decay; (ii) the case 3 does not consider the ternary fission contribution.

In summary, the TRANSURANUS fuel performance code satisfactorily agrees with the Monte Carlo depletion code VESTA for the UO_2 and MOX cases under consideration.

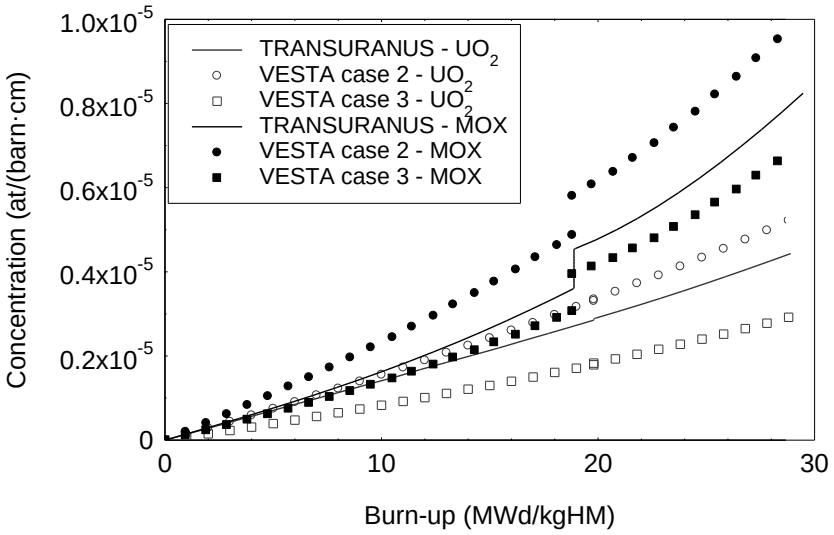

Figure 1.20 Comparison between the produced He computed by TRANSURANUS and by VESTA up to 30 MWd/kgHM.

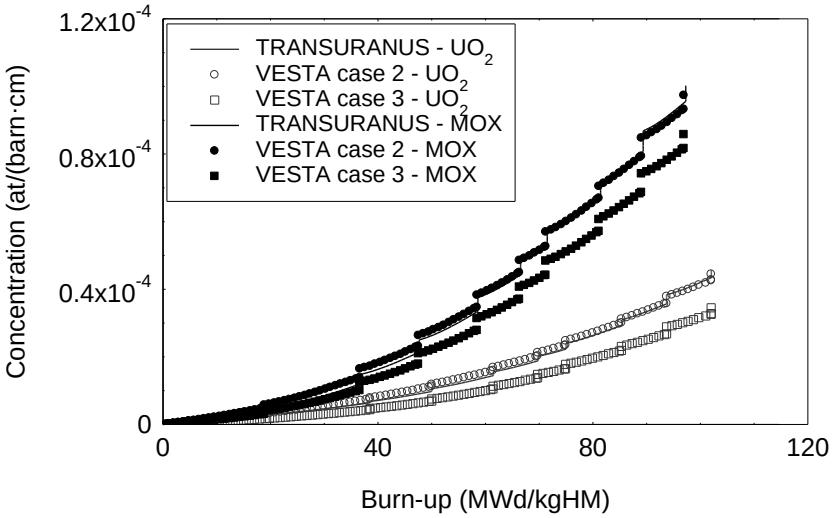

Figure 1.21 Comparison between the produced He computed by TRANSURANUS and by VESTA.

1.4 Model validation

The developed model has been validated on the basis of measured actinides and minor-actinides concentrations, since they are the main source of helium and since no experimental data are available for the helium created. Unlike classical burn-up analysis, where only average concentrations are of interest, the radial distribution inside the fuel pellet is of relevance in fuel performance evaluations. In fact, the behaviour of helium is strongly affected by the temperature, which varies across the fuel pellet.

For these reasons, the model validation has been divided in two parts. In the first part, average concentrations of fuels with a moderate burn-up (30-50 MWd/kgHM) measured by radiochemical techniques available in the SFCOMPO (Spent Fuel isotopic COMPOsition) database, developed by JAERI (Japan Atomic Energy Research Institute) and now managed by NEA (http://www.nea.fr/sfcompo/), have been compared with the model predictions. In the second part, normalized local concentrations across the fuel radius (radial profiles), measured at the Institute for Transuranium Elements, have been analysed for UO_2 fuels with a high burn-up (65-84 MWd/kgHM).

With increasing fuel burn-up the validation of simulated nuclide concentrations against experimental data is getting more and more challenging. Two issues should be emphasized for the analysis of the radial profiles:

- In current power reactors, very high burn-up can only be achieved in a small fraction of the loaded fuel rods that must be subject to non-standard irradiation configurations. For example, to generate a pellet-averaged burn-up in the order of 100 MWd/kgHM, the irradiation must cover at least 8 or 9 annual cycles and in this period the fuel rod has to be transferred several times into fuel assemblies with "fresh" neighbouring rods.

- To access the local nuclide concentrations across the radius of a fuel pellet, different experimental techniques with high spatial resolution have to be combined. A common approach is to apply wavelength dispersive electron probe microanalysis (EPMA) for determining element contents and secondary ion mass spectrometry (SIMS) for relative isotope concentrations. Moreover, the highly radioactive samples of irradiated nuclear fuel require sophisticated and tailored experimental installations (Walker, 1999; Desgranges et al., 2006a; Desgranges et al., 2006b).

As a consequence, the code validation cannot include all the quantities of interest. However, the comparison to simulations with more detailed and computation-intensive computer codes (in this case neutron transport calculations with the VESTA code, reported in the model verification) are a useful check, since these codes are on one hand cross-checked with the same measurements and on the other hand extensively validated on independent experimental data (Cousin et al., 2010)

1.5 Model validation with the SFCOMPO database

Among the different experimental data available in the SFCOMPO database, the Takahama-3 case (Nakahara et al., 2002) has been chosen since it is representative of a modern commercial PWR and since all the relevant radionuclides were available (Am, Cm, Pu and U isotopes).

Takahama-3 is a Japanese PWR with a typical 17x17 fuel assembly design (the main features are reported in Table 1.2). The samples were taken from two fuel assemblies. One was irradiated for two cycles and the other for three cycles. Three fuel pins were sampled at various axial locations, with one of these fuel pins being a burnable absorber. However, only the two UO_2 pins (called SF-95 and SF-97) have been considered for the present validation. In particular, five and six samples have been taken at different axial positions from the fuel rods SF-95 and SF-97, respectively.

In Figure 1.22, the power histories of the pins SF-95 and SF-97 are reported. In particular, in Figure 1.22a) and c), the maximum linear powers of the fuel rod SF-95 and SF-97 are shown, respectively. In Figure 1.22b) and d), the linear powers divided by the maximum value of the fuel rod are shown for the analysed samples as a function of the axial position. b) Refers to SF-95 and d) to SF-97. The values reported close to the symbols represent the burn-up (MWd/kgHM) reached by the sample.

The results are reported in Figure 1.23. a) to m), show the comparison between the measurements and the simulations with TUBRNP as a function of the burn-up of the eleven samples (i.e., five of SF-95 and six of SF-97). Concentrations of ^{241}Am, ^{243}Am,$^{238\text{-}242}$Pu, $^{242\text{-}245}$Cm, ^{235}U and ^{238}U are shown. Results are given in kg per tons of heavy metal initially loaded (kg/tHM). n) shows the histogram with the frequencies (not normalized) of relative errors of all the measurements, an average error of -0.5% with a standard deviation of 20% has been found.

Table 1.2 Data of fuel assemblies of Takahama-3 reactor.

Pellet	Initial composition (wt%)	^{234}U: 0.04 ^{235}U: 4.11 ^{238}U: 95.85
	Density (%TD)	95
	Diameter (mm)	8.05
Cladding	Material	Zircaloy-4
	Inner diameter (mm)	8.22
	Outer diameter (mm)	9.5
Fuel rod	Fuel stack length (mm)	3660
	Upper+lower plenum (mm)	≈170

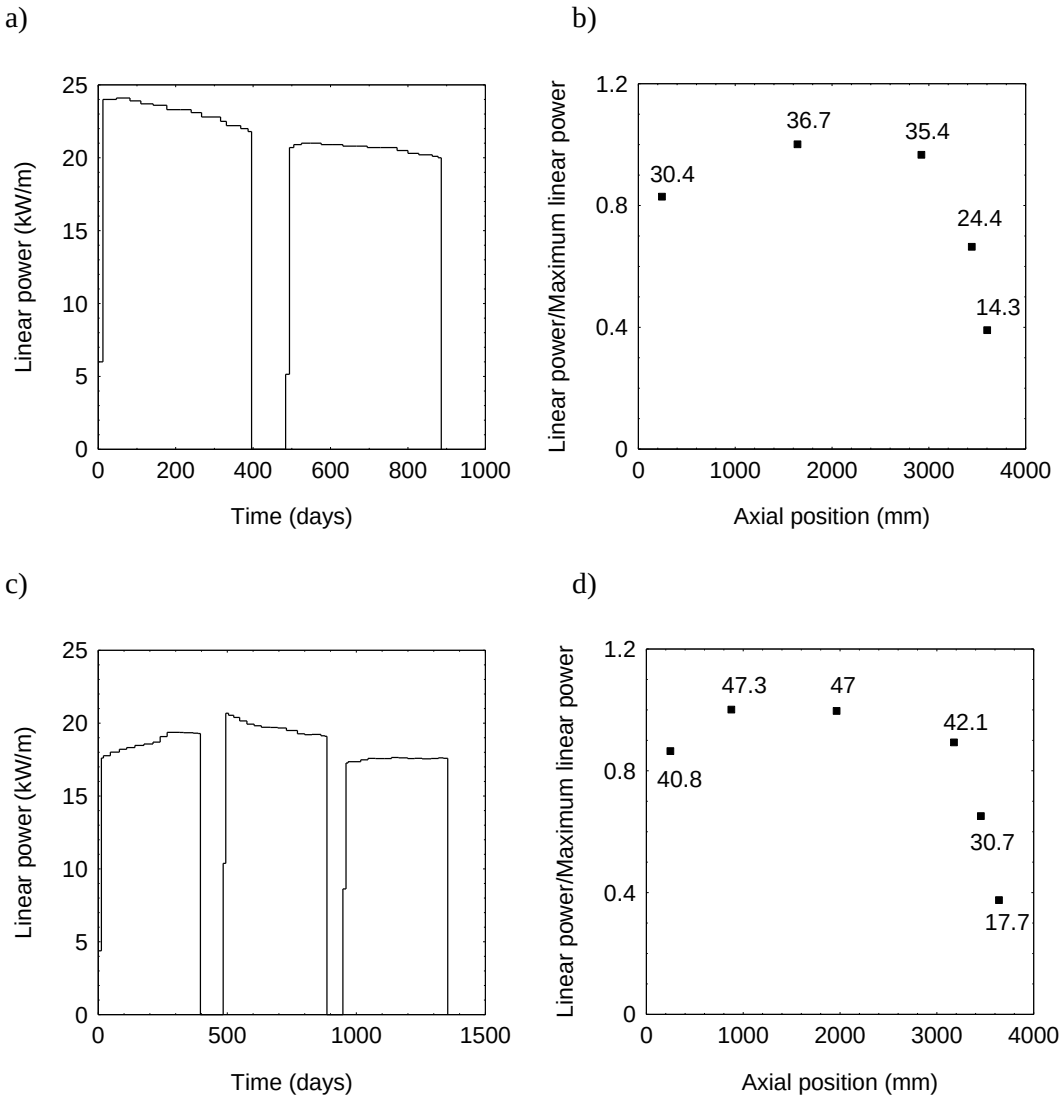

Figure 1.22 Power histories of fuel rods SF-95 and SF-97. a) and c): maximum linear power of the fuel rods SF-95 and SF-97, respectively. b) and d): linear power divided by the maximum value of the fuel rod for the analysed samples as a function of the axial position. b) Refers to SF-95 and d) to SF-97. The values reported close to the symbols represent the burn-up (MWd/kgHM) reached by the sample.

A good agreement can be seen. Some discrepancies exist, but (i) they are not far from the deviations obtained with more sophisticated neutron transport-depletion codes (see Kochunas, 2008; Nakahara et al., 2002), and (ii) are acceptable for the purpose of a fuel performance code, especially in view of the uncertainties related to the behaviour of the helium in the fuel. It is also important to point out that no uncertainties of the measurements are reported in the SFCOMPO database, but they should be taken into account for a better interpretation of the comparison with the simulations.

a)

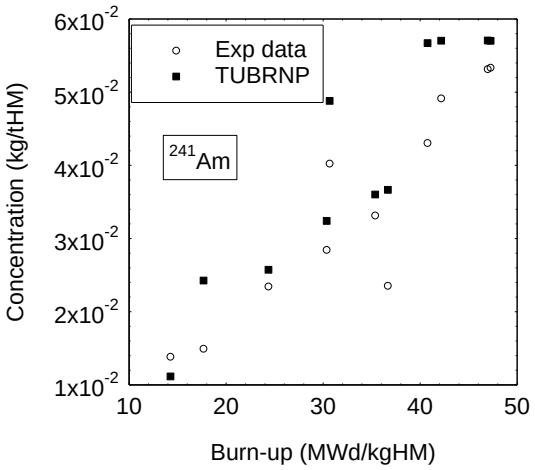
Exp data
TUBRNP
241Am
Concentration (kg/tHM)
Burn-up (MWd/kgHM)

b)

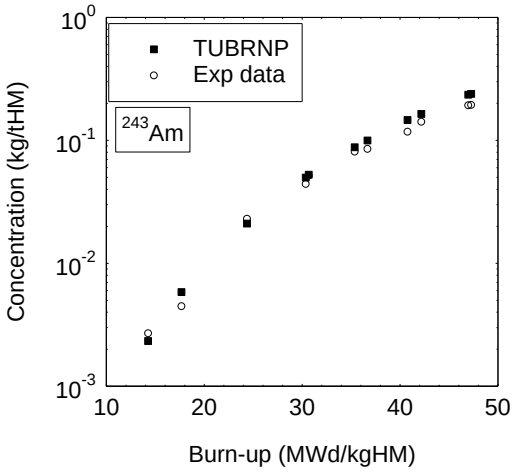
TUBRNP
Exp data
243Am
Concentration (kg/tHM)
Burn-up (MWd/kgHM)

c)

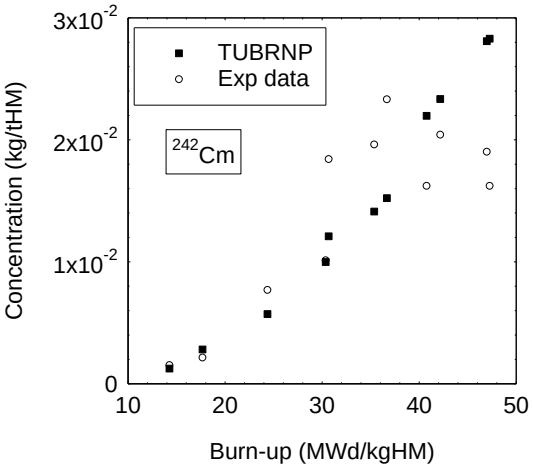
TUBRNP
Exp data
242Cm
Concentration (kg/tHM)
Burn-up (MWd/kgHM)

d)

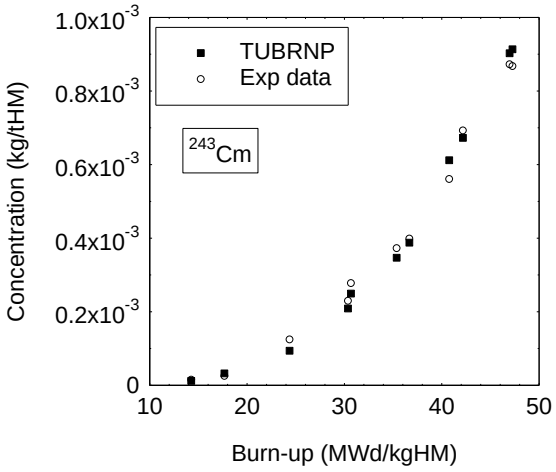
TUBRNP
Exp data
243Cm
Concentration (kg/tHM)
Burn-up (MWd/kgHM)

e)

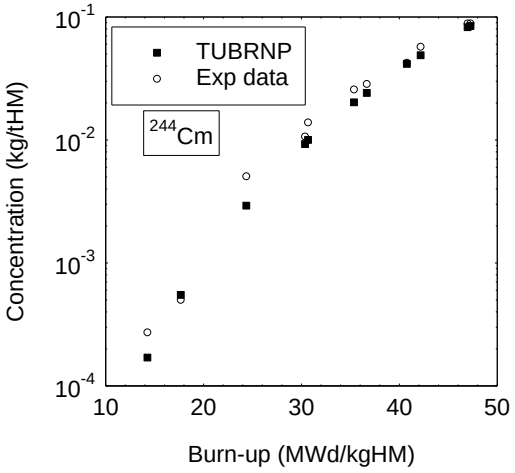
TUBRNP
Exp data
244Cm
Concentration (kg/tHM)
Burn-up (MWd/kgHM)

f)

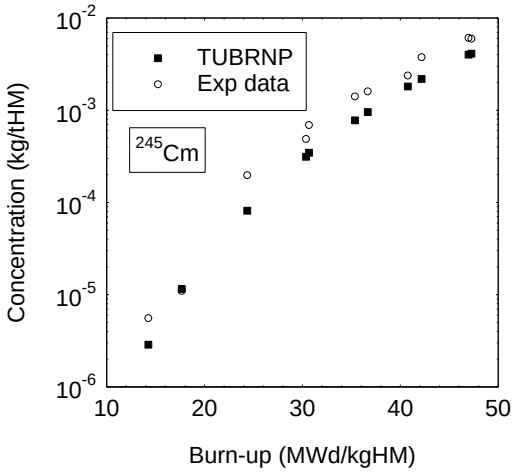
TUBRNP
Exp data
245Cm
Concentration (kg/tHM)
Burn-up (MWd/kgHM)

g)

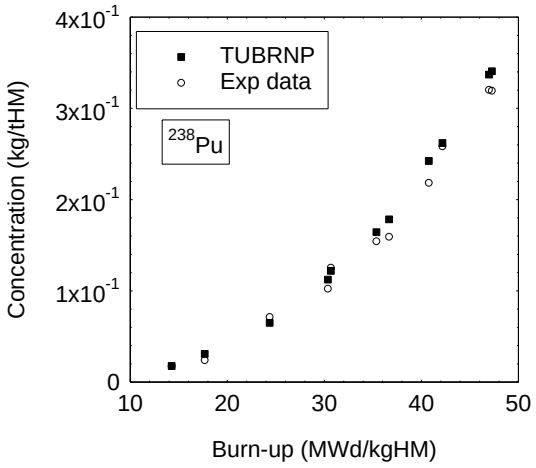
TUBRNP
Exp data
238Pu
Concentration (kg/tHM)
Burn-up (MWd/kgHM)

h)

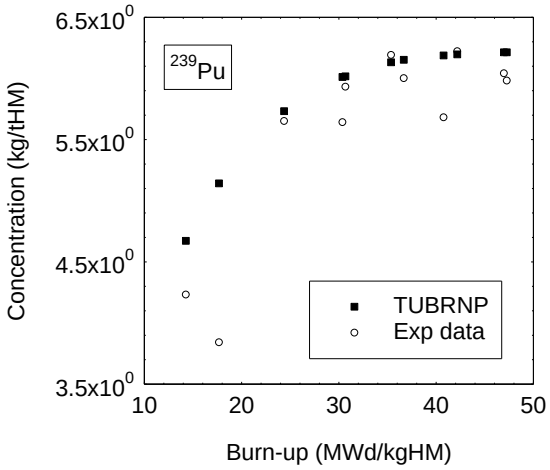
239Pu
TUBRNP
Exp data
Concentration (kg/tHM)
Burn-up (MWd/kgHM)

i)

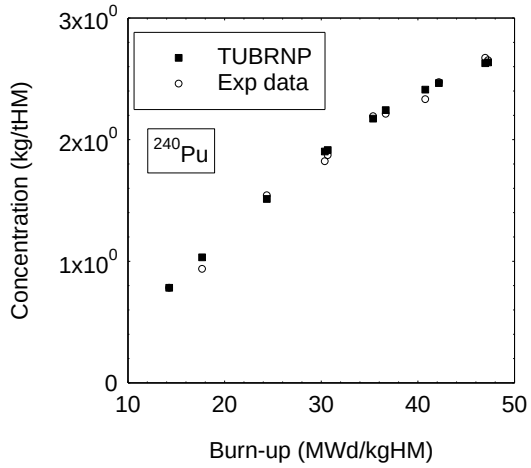
TUBRNP
Exp data
240Pu
Concentration (kg/tHM)
Burn-up (MWd/kgHM)

j)

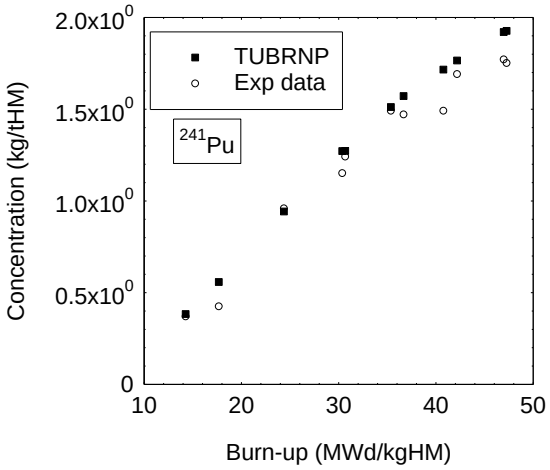
TUBRNP
Exp data
241Pu
Concentration (kg/tHM)
Burn-up (MWd/kgHM)

k)

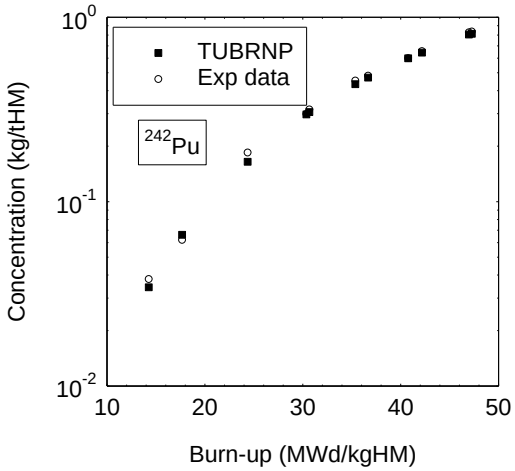
TUBRNP
Exp data
242Pu
Concentration (kg/tHM)
Burn-up (MWd/kgHM)

l)

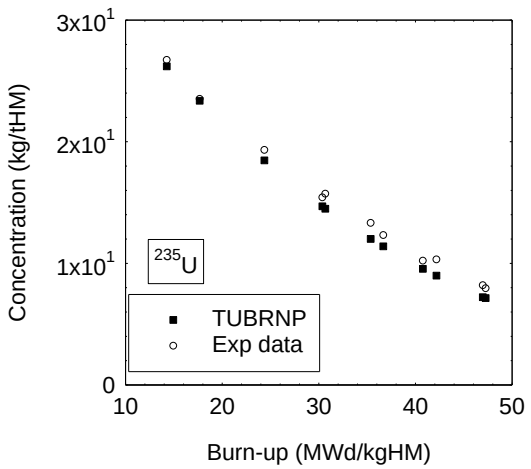
235U
TUBRNP
Exp data
Concentration (kg/tHM)
Burn-up (MWd/kgHM)

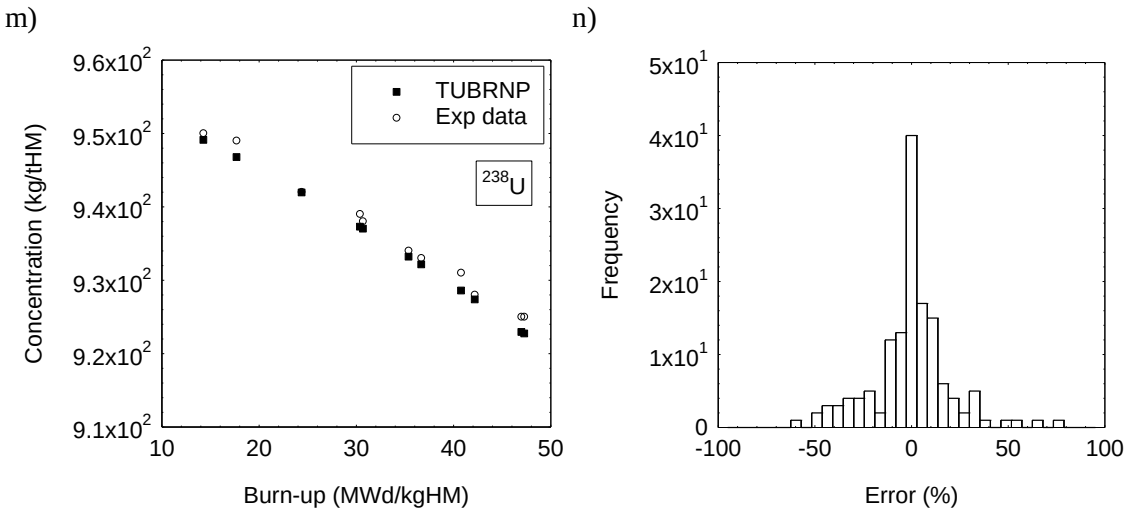

Figure 1.23 a) to m): comparison between the measurements and the simulations with TUBRNP as a function of the burn-up of the eleven samples (i.e., five of SF-95 and six of SF-97). ^{241}Am, ^{243}Am, $^{238\text{-}242}$Pu, $^{242\text{-}245}$Cm, ^{235}U and ^{238}U are shown. n): histogram with the frequencies (not normalized) of relative errors of all the measurements.

1.6 Model validation with ITU data

1.6.1 Experimental data

For the present work, microscopic measurements of two samples of irradiated UO_2 fuel with an initial enrichment of 3.5 wt.% ^{235}U and a pellet diameter of 9.3 mm, have been used. The data have been obtained by EPMA (measuring the local concentrations of Pu and Nd), and by SIMS (determining the normalized local nuclide concentrations), as summarized in Table 1.3. More details about the specific application of these experimental techniques can be found in (Walker, 1999; Walker et al., 2009).

Both fuel rods have been irradiated in a typical 15x15 fuel assembly of a commercial PWR. For sample #1(12H3-LP), the power history (both rod average and at the sample position, 31 cm from the bottom end) is given in Table 1.4 for each cycle together with the evaluated burn-up. For sample #2 (14D8), the average power levels at the sample position (2903 mm from the bottom of the fuel stack) are listed in Table 1.5 for each cycle together with the evaluated burn-up. It is worth mentioning that the power histories are spanned in 7 and 8 reactor cycles in order to reach such high burn-ups.

1.6.2 Comparison with the experimental data

Figure 1.24 shows the radially averaged total Pu concentrations measured for irradiated slices of UO_2 fuel considered in (Schubert et al., 2008), together with the measurements

of the two samples introduced in this section (red full triangles) and with the total measurements of the Takahama-3 reactor (orange full circles).

Table 1.3 Samples of irradiated UO_2 analysed.

Sample ID	Slice-average burn-up (MWd/kgHM)	Analytical technique	Measured concentrations	Number of radial positions
1 (12H3-LP)	65	EPMA	Pu and Nd (wt. %)	44 + 21*
		SIMS	^{239}Pu, ^{240}Pu, ^{242}Pu, ^{241}Pu+^{241}Am, ^{243}Am, ^{244}Cm (normalized)	32
2 (14D8)	81	EPMA	Pu and Nd (wt. %)	44

*Second set of measurements covering the fuel periphery from approx. 93% of the total fuel radius

Table 1.4 Power history and computed burn-up evolution of the rod 12H3-LP at the sample position.

Annual Reactor cycle	Linear heat generation rate at the sample position (rod average) (kW/m)*	Computed burn-up at the sample position (rod average) (MWd/kgHM)
1	24.5 (34)	13.8 (19)
2	20.9 (29)	26.8 (37)
3	16.6 (23)	34.8 (48)
4	14.4 (20)	42.8 (59)
5	13.0 (18)	48.6 (67)
6	12.2 (17)	52.2 (72))
7	11.5 (16)	59.4 (82)
8	10.1 (14)	65.2 (90)

These measurements are compared with the predictions of both the new extended version of TUBRNP and VESTA. Since the dataset of effective cross sections in TUBRNP does not include specific values for a 3.5% enriched UO_2 fuel, the effective cross sections for an initial enrichment ($^{235}U/^{tot}U$) of 4% (curve a) and 3% (curve b) have been applied. The Pu evolution as a function of the burn-up is slightly different for

the two codes, due to the differences between the one-group effective cross sections implemented in TRANSURANUS and those evaluated by VESTA. Moreover, the effective cross sections of TRANSURANUS are not dependent on time. However, both predictions of the total Pu concentration lie within the scatter of the experimental data, except for the low total Pu concentration measured in sample #1 (12H3-LP), which needs further consideration. It could be explained by the bottom-end position of the sample and by the repeated re-positioning of the fuel rod during the eight annual irradiation cycles, implying that the neutron spectrum was not completely representative of the average conditions of the reactor. However, no detailed information is available to draw a definitive conclusion.

In view of the limited available information on the detailed irradiation conditions, normalized radial distributions are used for the comparison of the measured and calculated local concentrations. For both samples, EPMA measurements of local Nd concentrations (which give an indication of the local burn-up) and local Pu concentrations are shown in Figure 1.25. The comparison with the corresponding simulations by TUBRNP reveals a good agreement. For sample #1, SIMS measurements of all relevant Pu, Am and Cm nuclides for the helium production are available and can be compared with the simulations of both TUBRNP and VESTA (Figure 1.26). As the SIMS technique cannot distinguish between different nuclides of the same mass number, the sum of the concentrations of ^{241}Pu+^{241}Am is analysed, and ^{238}Pu and ^{242}Cm cannot be revealed, since hidden by ^{238}U and ^{242}Pu, respectively. The agreement between both types of simulations on one hand, and the experimental data on the other hand, is very satisfactory.

Table 1.5 Power history and computed burn-up evolution of the rod 14D8 at the sample position.

Annual Reactor cycle	**Linear heat generation rate at the sample position (kW/m)***	**Computed burn-up at the sample position (MWd/kgHM)**
1	31.1	16
2	26.2	30
3	21.7	41
4	18.1	51
5	20.2	62
6	18.4	72
7	15.6	81

* Average value during the reactor cycle

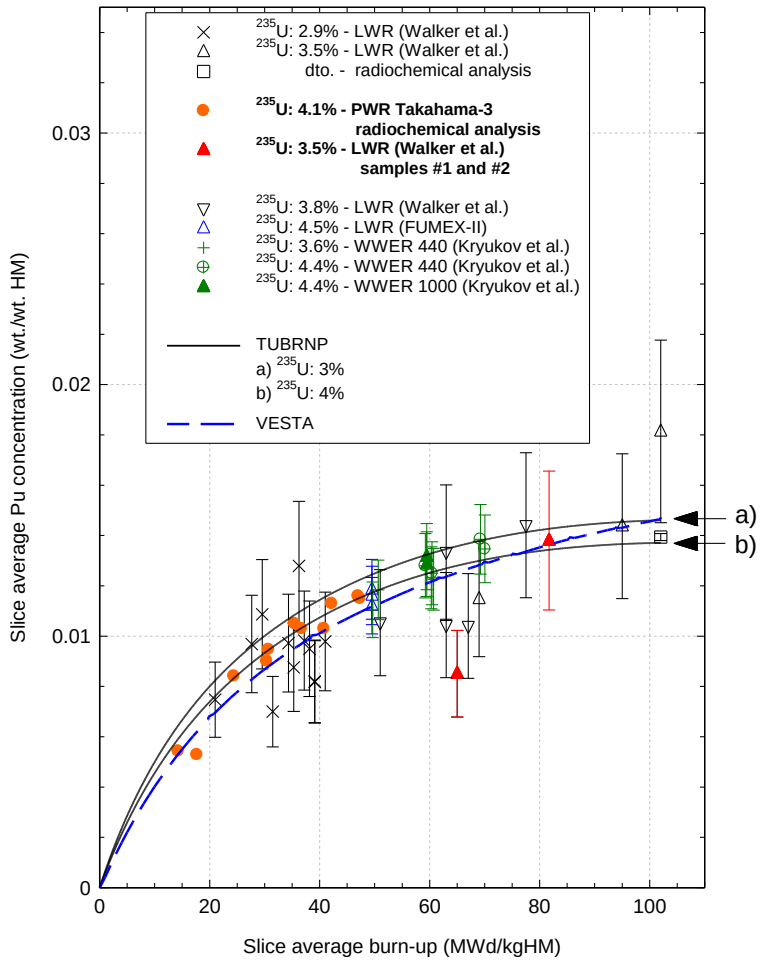

Figure 1.24 Slice-average total plutonium concentration as calculated by TUBRNP (full lines) and by VESTA (dashed line) for a 3.5% enriched UO_2 fuel, compared with EPMA measurements of irradiated UO_2 fuel (Lassmann et al., 1994; Manzel and Walker, 2000; Sontheimer and Landskron, 2000; Manzel and Walker, 2002; Kryukov et al., 2006; Killeen et al., 2007) with enrichments ranging from 2.9 to 4.5%. Since the dataset of effective cross sections in TUBRNP does not include specific values for a 3.5% enriched UO_2 fuel, the results are based on the effective cross sections for an initial enrichment ($^{235}U/^{tot}U$) of 4% (curve a) and 3% (curve b).

It is interesting to note that only the local concentration of ^{240}Pu is sufficiently sensitive to the form factor for resonance absorption in ^{240}Pu. For the sake of completeness, coefficients p_2 and p_3 in equation (1.4) have been fitted to the data for UO_2 obtaining p_2=1.0 and p_3=0.65. These values have subsequently been used for the simulation of the relative radial profile of ^{240}Pu in MOX fuel published by Bart et al. (1994). The results

are plotted in Figure 1.27 and show that the values of p_2 and p_3 fitted for UO_2 are not suitable for the MOX fuel under consideration. Accordingly, a fit of p_2 and p_3 should be carried out for each case specifically. Furthermore, the impact of p_2 and p_3 is negligible for the other nuclides. Considering the limited improvement for the relative radial profile of ^{240}Pu, the negligible impact on the main outcome of TUBRNP (which is the relative power profile and the helium production), the large uncertainties on the mobility of He that is necessary to predict its release, and finally the increase of the required computational costs, the fit of p_2 and p_3 for each fuel and reactor type is not recommended for the application of TUBRNP.

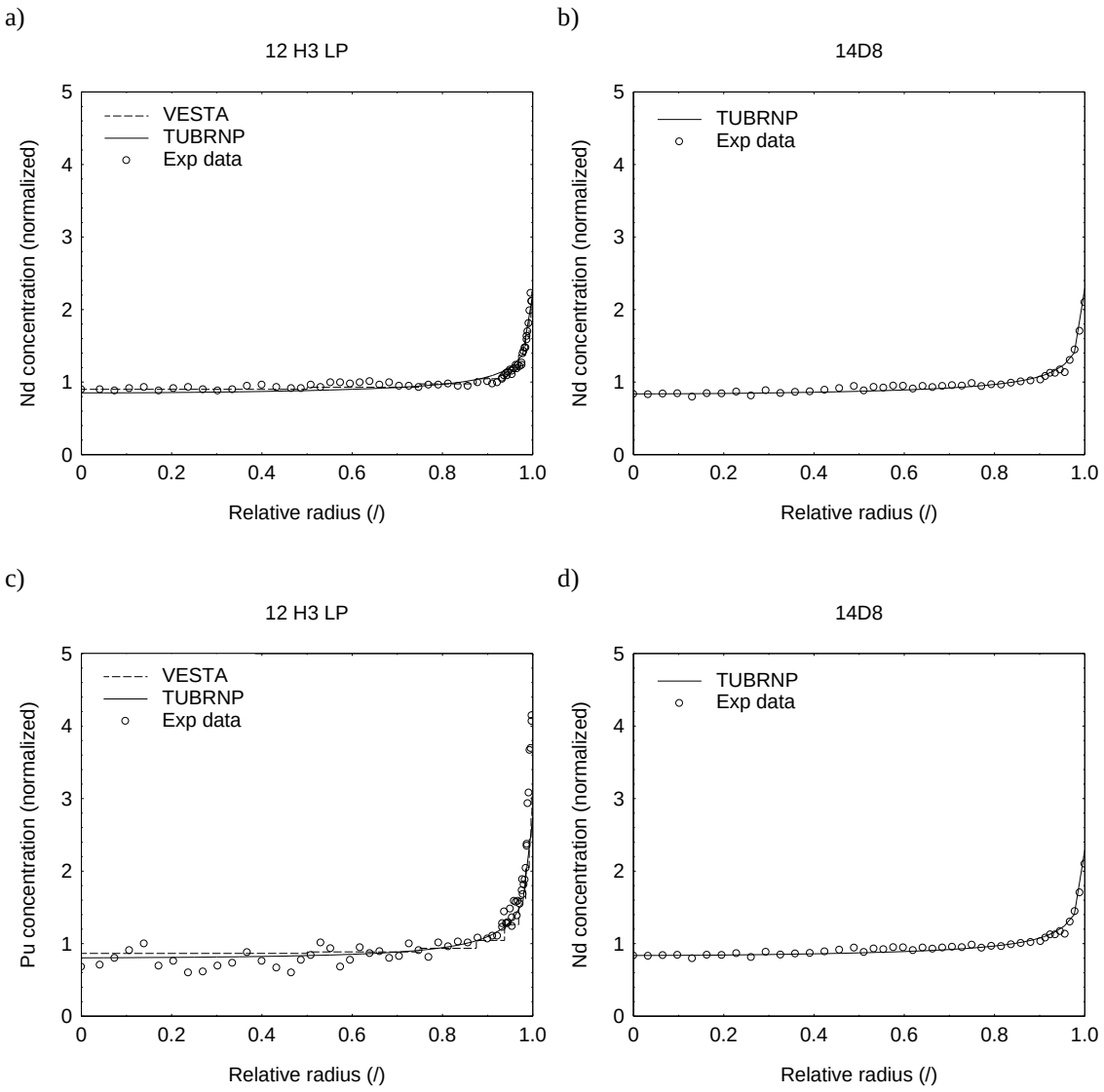

Figure 1.25 Radial distribution of the normalized Nd (top) and Pu content (bottom) calculated by TUBRNP and compared with EPMA measurements for samples #1(12H3-LP) and #2(14D8).

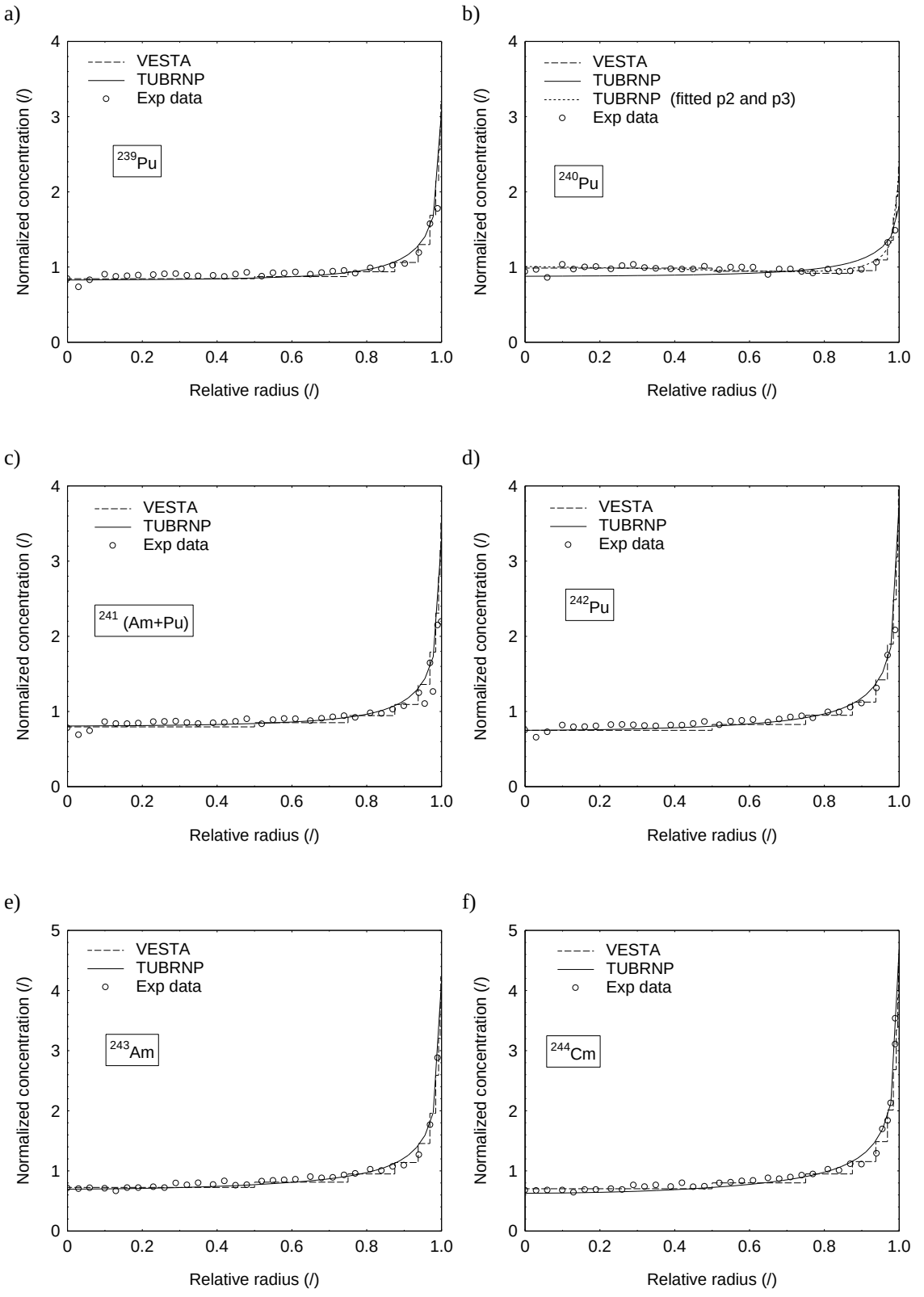

Figure 1.26 Normalized radial distribution of the local concentrations of ^{239,240}Pu, ^{241}Pu+^{241}Am, ^{242}Pu, ^{243}Am, and ^{244}Cm in irradiated UO_2, calculated by TUBRNP (sample #1/12 H 3-LP). The results are compared with SIMS measurements (markers) and with simulations by the VESTA code (dashed lines).

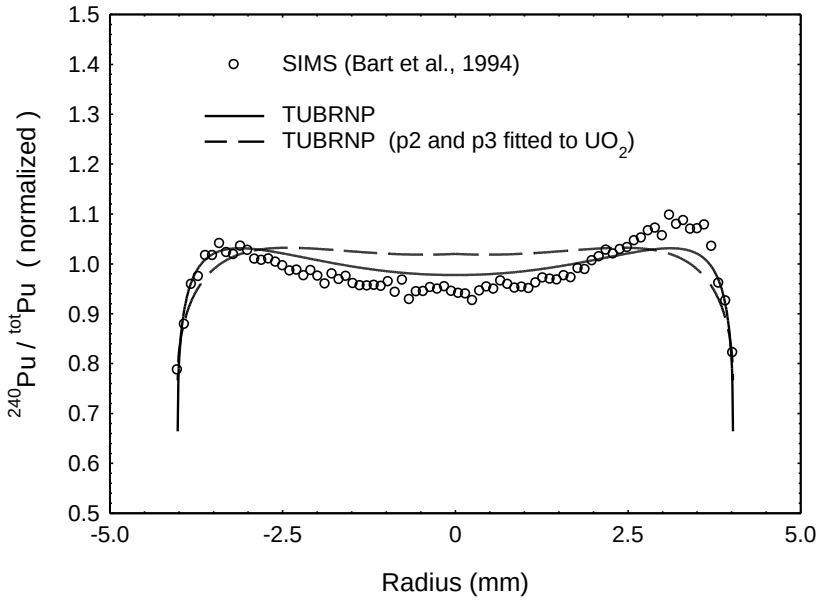

Figure 1.27 Normalized radial distribution of the local concentrations of ^{240}Pu in irradiated MOX calculated by TUBRNP for two sets of the p_2 and p_3 parameters in the form factor $f_{240Pu}(r)$, and SIMS measurements (markers) published by Bart et al. (1994).

Figure 1.28 shows a comparison between the helium production simulated for sample #1 in two extreme situations: (i) with long shut down periods (200-250 days) between the different irradiation cycles, and (ii) with short shut down periods (30 days). The length of the shut down periods influences the total helium content, as shown in Figure 1.28a. This figure also reveals that the prediction for both codes is in good agreement. The difference is mainly due to the (n,α) contribution. In fact the JEFF 3.1 library has a ^{16}O(n,α)^{13}C cross section overestimated of about 40% as already discussed in the previous sections.

The shutdowns are expected to affect also the radial profiles of ^{4}He. Indeed, the radial profile of the (n,α) contribution is almost flat and that of the ternary fission contribution follows the power radial profile, whereas the α decay contribution depends on the radial profiles of ^{242}Cm, ^{244}Cm and ^{238}Pu. Moreover, the average evolution of the first two terms depends on the burn-up, while the α decay depends on the time. For the two extreme cases considered, Figure 1.28b shows that the resulting difference in the radial profile of the total concentration of ^{4}He is very small and that the effect is consistently simulated by TUBRNP and VESTA.

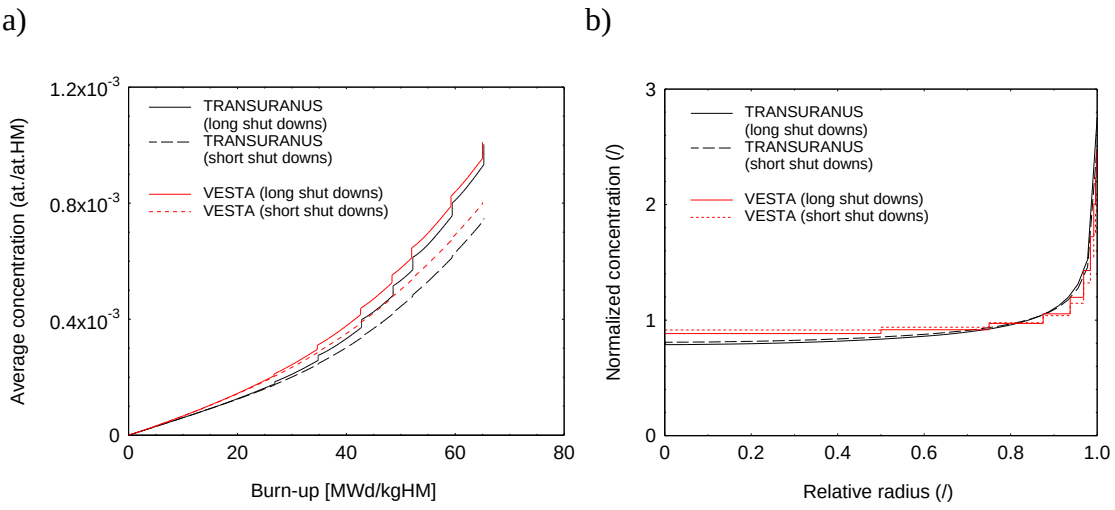

Figure 1.28 Produced ^{4}He in irradiated UO_2 (sample #1/12H3-LP) calculated by TRANSURANUS and VESTA: average concentration a) and normalized radial distribution b), the influence of the shut down length is shown.

1.7 Summary and concluding remarks

In the present chapter, a model for the production of helium, which has been developed and implemented in the TRANSURANUS fuel performance code, is presented.

The model parameters have been evaluated on the basis of information available in literature (nuclear data) and on the basis of MCNP simulations (cross sections).

The models and the evaluated parameters have been verified on the basis of the Monte Carlo depletion code VESTA. A typical power history extended to a burn-up of 100 MWd/kgHM has been simulated for two selected PWR fuel compositions (MOX and UO_2). As a first step of the verification of the helium production model, a satisfactory agreement between the flux computed by the formula adopted in the model and the values obtained directly by VESTA has been found. This agreement has been improved by including the concentrations of further fissile and fissionable nuclides, which become important at high burn-up.

The following conclusions can be drawn from the comparison between TRANSURANUS and VESTA simulations:

- The set of equations implemented in TUBRNP, refined in the present work, are sufficient to correctly describe the evolution of the nuclides that are relevant for power and helium generation in UO_2 and MOX fuels.

- By considering the set of data already present in the code (capture and fission cross sections of the actinides), together with the new evaluated ones (ternary fission yield, $^{16}O(n,\alpha)^{13}C$ cross section, branching ratios of the $^{241}Am(n,\gamma)^{242m}Am$ reaction and of the ^{242}Am decay due to electron capture), the agreement with helium concentrations simulated by the VESTA code is very satisfactory.

As a final step, the validation of the model has been based on (i) average concentrations of actinides, available in the SFCOMPO database and (ii) radial profiles of relevant elements/nuclides from EPMA and SIMS available at JRC/ITU. The latter have also been used to extend the validation of the VESTA code. A good agreement has been found with the experimental data, covering average concentrations of Am, Cm, Pu and U isotopes, relative radial profiles of Pu and Nd concentrations measured by EPMA and relative radial profiles of $^{239-240}Pu$, $^{241}Pu+^{241}Am$, ^{242}Pu, ^{243}Am and ^{244}Cm measured by SIMS.

In conclusion, the developed model offers several advantages: (i) it gives reliable predictions (within the uncertainty related to the cross section libraries) in a short computational time, for typical LWR fuel rods, both in terms of average concentration and radial profiles; (ii) it can be easily coupled with a model for the helium release, since it is integrated in a fuel performance code; (iii) although developed for LWR conditions, it can be easily extended to other reactors (e.g., fast reactors, where the higher content of plutonium and the possible presence of americium in the fuel can lead to a larger production of helium).

Further microscopic experimental data are required for a more detailed evaluation of the prediction capability of the model. The local concentration of helium across a fuel rod is obviously most relevant, in particular for MOX fuels due to the higher helium generation rate. In the absence of available He data, measurements of the local concentrations of Pu, Am and Cm nuclides should be analysed, and are in any case needed for a complete validation of the model. Moreover, for both UO_2 and MOX, a comprehensive code validation will require a comparison with measurements of absolute concentrations of Am, Cm, and He at high burn-ups.

When interpreting the measured He concentrations, one must carefully address their variation in space and time, because of (i) a rapid migration of the light He atoms and (ii) the time dependence of the He content due to its build-up from decay of ^{242}Cm, ^{244}Cm and ^{238}Pu.

It is still an open question to which extent the local concentration of He and its variations influence the local material properties within a fuel rod, e.g. the local thermal conductivity. In any case, a correct prediction of the produced helium according to the model is the first step for predicting the amount of helium released in the gap between the fuel and the cladding or trapped within the fuel. This aspect is important for fuel

performance simulations in view of increasing discharge burn-up values, linear heat generation rate, Pu and minor actinide contents. It is also essential when simulating long term storage of conventional and advanced nuclear fuels.

Chapter 2
Helium behaviour and release

Due to the low solubility and high diffusion coefficient, helium can be easily released in the gap between the fuel and the cladding. However, if the helium initially loaded in the gap is at a sufficient high pressure, the release of the amount created in the fuel can be inhibited, and part of the helium in the gap can even be absorbed by the fuel. Predicting the amount of helium released in the gap and the amount trapped in the fuel is of relevance. In fact, helium in the fuel can contribute to fuel swelling and to the degradation of the thermal conductivity, while the helium released can enhance the fuel rod inner pressure, with important consequences for the safety.

In this chapter, a model for the release of helium in oxide fuels is discussed. The model has been implemented in the TRANSURANUS code, coupled with the helium production and grain growth models, and preliminarily validated on the basis of pressurized and unpressurized fuel rods.

The chapter is structured as follows. In the first section, a review of current modelling of helium behaviour in fuel performance analysis is discussed. In the second section, a model for the release and absorption of helium is proposed. In the last section, the model is independently tested on irradiation histories.

2.1 Available models for helium release in LWR oxide fuels

In this section, a review of the approaches adopted in the open literature for treating the helium release in oxide fuels is reported.

The simplest approach is the previous approach of TRANSURANUS, where the release is assumed as a constant fraction (user defined) of the total produced helium (TRANSURANUS, 2009).

Since the production of helium is low compared to the amount of fission gases (xenon and krypton) generated, some authors suggest that helium can be released only once the fission gas bubbles interconnect (Hodge et al., 2005; Federici et al., 2007; Katsuyama et al., 2010). For this reason, they suppose that in case of unpressurized rods (i.e., when absorption can be neglected) it should be linked to the fission gas release. In Figure 2.1, released helium measured in unpressurized MOX fuel rods (BWR (Kamimura et al., 1999), FBR (Katsuyama et al., 2010), ATR (Hodge et al., 2005)) are reported as a function of the fission gas release, and compared with the curves proposed by Federici and co-authors (Federici et al., 2007).

Since the solubility of helium is low (Federici et al., 2007; Maugeri et al., 2009), Federici and co-authors assumed that the grain boundary would work as a perfect sink, as in the case of fission gases. Hence, by solving the diffusion equation in a sphere with homogeneous Dirichelet boundary conditions, under constant conditions (i.e., constant temperature and domain volume), the amount of fission gases leaving the domain divided by the amount of gas generated can be expressed by (Booth, 1957):

$$f(\tau) = 1 - \frac{1}{15\tau}\left(1 - 90\sum_{n=1}^{\infty}\frac{\exp\left(-n^2\pi^2\tau\right)}{n^4\pi^4}\right) \tag{2.1}$$

where τ is an equivalent time defined as:

$$\tau = \frac{D_{eff}}{a^2}\cdot t \tag{2.2}$$

D_{eff} is an effective diffusion coefficient that takes into account trapping and resolution[1] (Speight, 1969), a is the radius of the equivalent sphere and t the real time.

The short time approximation can be expressed as:

$$f(\tau) = 4\sqrt{\frac{\tau}{\pi}} \tag{2.3}$$

[1] During their Brownian motion, atoms of gases with a low solubility (e.g., Xe, Kr, He) can be trapped (i.e., precipitate) in bubbles. On the other hand, fission spikes can interact with the bubbles and resolute the gas atoms into the solid matrix (i.e., in solution).

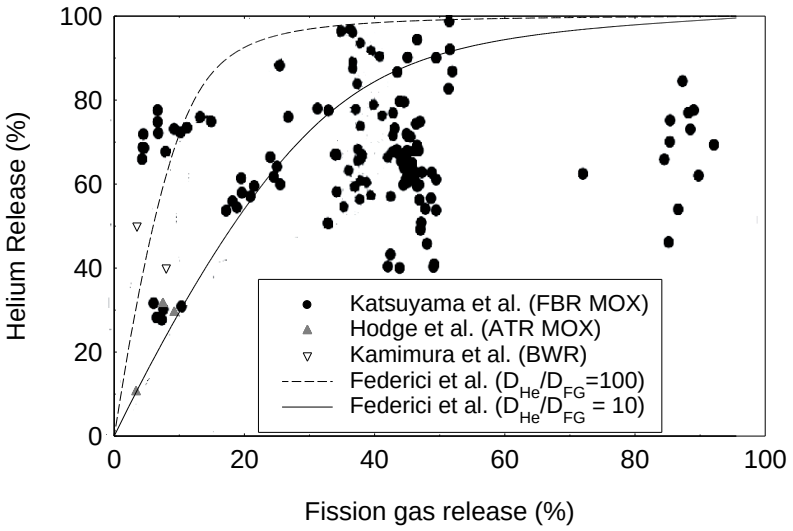

Figure 2.1 Fractional helium releases as a function of the fractional fission gas release for unpressurized fuel rods.

Federici and co-authors assumed that the ratio between the helium effective diffusion coefficient and that of fission gas is between 10 and 100. The curves reported in Figure 2.1 represent $f(\tau \cdot 10)$ as a function of $f(\tau)$ and $f(\tau \cdot 100)$ as a function of $f(\tau)$. However, the assumption of a factor 10 to 100 between the diffusion coefficients seems an adaptation in order to find a factor between 3 and 10 in terms of fractional releases, in accordance with the experimental evidences. In fact, by using the short time approximation, the fractional releases are proportional to the square root of the diffusion coefficient.

The thermal diffusion coefficients of helium reported by Federici and co-authors, which refer to both ion implantation and infusion experiments by different authors (Bostrom, 1958; Rufeh et al., 1965; Sung, 1967; Guilbert et al., 2004; Roudil et al., 2004; Blanpain et al., 2006), are quite dispersed, meaning that they do not reflect a simple volume diffusion. They are rather representative of an effective behaviour depending on the experimental conditions and the way the results are interpreted. However, they are confined between the following relations, which are valid in the range (800°C, 1500°C):

$$\begin{aligned} D_{He,\min} &= 8.887 \cdot 10^{-14} \cdot \exp(-17505.9/T) \\ D_{He,\max,NoR} &= 2.222 \cdot 10^{-11} \cdot \exp(-17505.9/T) \end{aligned} \qquad (2.4)$$

In these expressions, the diffusion coefficients are in (m^2/s), and T (K) is the absolute temperature. By dividing these equations by the thermal diffusion coefficient of Xe provided by Matzke (1980), we found a ratio quite different with respect to the factor 10-100 suggested by the authors (Figure 2.2). However, they do not indicate which fission gas diffusion coefficient they used. It is worth noting that the migration energy of Xe and He are quite different, meaning that the ratio of the diffusion coefficients of

He and Xe strongly depends on the temperature, and a simple factor cannot be representative of the whole temperature range inside a fuel pellet.

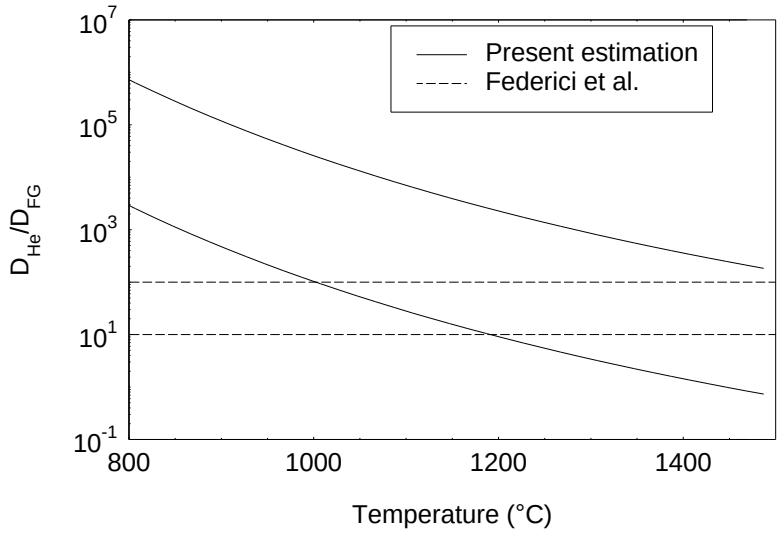

Figure 2.2 Ratio between the thermal diffusion coefficient of helium and fission gases.

On the other hand, Kamimura et al. (1999) assumed a ratio between the diffusion coefficient of helium and fission gases of 1000. Considering the short-time approximation, this means that the helium release should be 30 times larger than fission gas release. Since in contradiction with the experimental evidences (where helium fractional releases are 3 to 10 the fission gas releases), they argued that at the boundary area, grain boundary bubbles are small, and frequent exchange of gas atoms between matrix and bubbles caused by trapping by fission gas bubbles and re-solution by fission fragments makes the proportion of helium to fission gases in the bubbles the same as that in the matrix. This means that helium and fission gas volumes on the grain boundary (and/or in the matrix) are proportional to each generation, and the proportion of helium to fission gas in each area coincides to that of its yield.

Kurita and co-authors (Kurita et al., 1999) showed their results in terms of volume of helium released as a function of volume of fission gas released. These data refer to MOX fuels irradiated in the Advanced Test Reactor FUGEN in Japan. A clear correlation can be seen in Figure 2.3a. However, when including the data of the ATR irradiation test and of Kamimura and co-authors the dispersion increases. In Figure 2.3b, a rough estimation of the data of Katsuyama and co-authors (which refer to FBR conditions) is reported and compared with the other data. It is important to mention that

the data of Katsuyama and co-authors are actually quite dispersed, especially in the region around 500 cm^3/ $kg_{fuel}$of released fission products[2].

In the open literature, it is also possible to find a model developed by Ronchi and Hiernaut (Ronchi and Hiernaut, 2004) used for interpreting helium release curves of experiments conducted in Knudsen cells. They modelled the helium behaviour by means of three reaction rate equations:

$$\begin{aligned}
\frac{dg_{sol}}{dt} &= -K_{RH}\, g_{sol} - \left(H_{RH} + S_{RH}\right) g_{sol} \\
\frac{dg_{trap}}{dt} &= K_{RH}\, g_{sol} - U_{RH}\, g_{trap} \\
\frac{dg_{rel}}{dt} &= \left(H_{RH} + S_{RH}\right) g_{sol} + U_{RH}\, g_{trap}
\end{aligned} \qquad (2.5)$$

where g_{sol} is the amount of gas in solution, g_{trap} the amount trapped, and g_{rel} the amount released, K_{RH} is the trapping rate, H_{RH} a de-sorption rate proportional to the trapping, S_{RH} a pure de-sorption rate, U_{RH} the release rate of the amount trapped. However, these coefficients are not known a priori, and the values fitted on the basis of the release curves were quite different for the different samples. For this reason, this model has been disregarded.

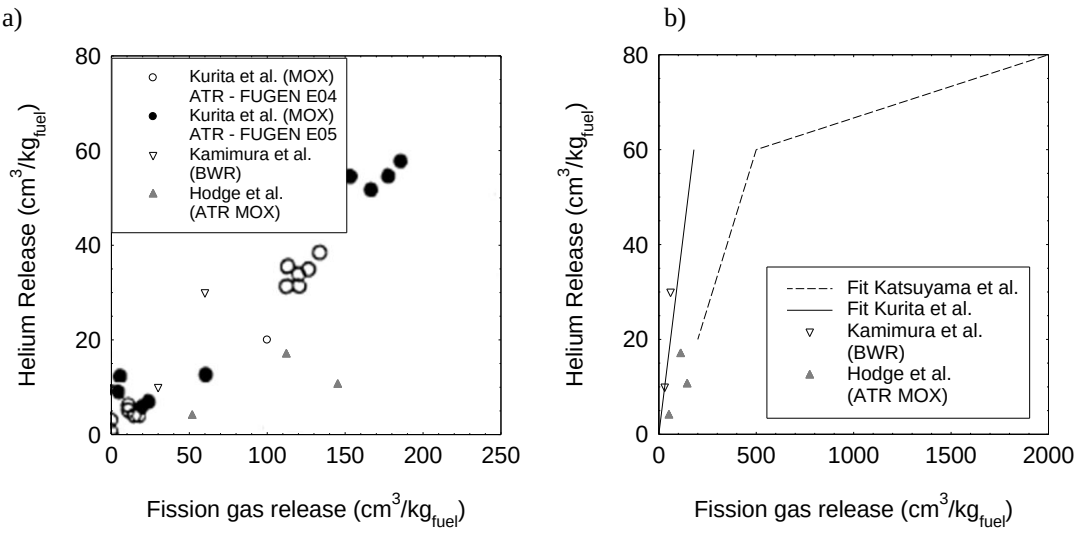

Figure 2.3 Amount of helium released as a function of amount of FG released: a) LWR conditions, b) comparison between LWR and FBR conditions.

[2] Throughout the chapter, the volume of gas (cm^3) refers to the Standard Temperature and Pressure (STP) conditions.

As far as the absorption mechanism is concerned, the only work describing a possible approach is the one of Federici and co-authors. They assumed that the thermodynamic equilibrium induced by the thermal resolution is reached when the He partial pressures in the inter-granular cavities and in the free volume are equal. The molar concentration of He can then be calculated, according to the ideal gas law, considering the free volume He partial pressure (hot conditions) and the volume fraction of inter-granular cavities. In order to calculate the kinetics associated with this mechanism, they suggest that one can replace the grain boundary "lattice", along which He is diffusing and being trapped, by a homogeneous volume of the equivalent sphere representing the fuel fragment. Introducing the grain boundary equivalent time (τ_{GB}), defined by using a grain boundary effective diffusion coefficient, the analytical expression for the calculation of the kinetics can be written as:

$$C_{He}(\tau_{GB}) = C_{He,eq}\left(1 - \frac{6}{\pi^2}\sum_{n=1}^{\infty}\frac{\exp\left(-n^2\pi^2\tau_{GB}\right)}{n^2}\right) \tag{2.6}$$

where τ_{GB} is an equivalent time defined as:

$$\tau_{GB} = \frac{D_{eff,GB}}{a^2}\cdot t \tag{2.7}$$

where $D_{eff,GB}$ is an equivalent grain boundary diffusion coefficient, a the equivalent sphere diameter and t the real time. However, they do not discuss the values of the parameters of the model. The only indication is that empirical evidences seem to indicate that the equilibrium in the inter-granular cavities is reached after one reactor irradiation cycle.

In Figure 2.4, experimental data of released helium measured in PWR reactors reported by Barker et al. (2006) are shown. They refer to SBR MOX fuels irradiated in the Beznau-1 reactor in Switzerland. An infusion of helium can be seen for low burn-up, but a release is achieved for higher burn-ups. Although not reported, the uncertainty of these data should not be negligible. In fact, this is the sum of the uncertainty of the moles measured after the irradiation plus the uncertainty of the moles initially loaded. An uncertainty of ±5% is reported by Hodge et al. (2005) for the fraction of helium (i.e., moles of helium divided by the total number of moles) in the free volume of the ATR rods, measured by mass spectrometry. By considering the geometry and initial pressure of these rods, it is possible to estimate about $1.5\cdot10^{-2}$ moles initially loaded, meaning 335 cm^3 STP at 273 Kelvin. This means that even an uncertainty of ±1% (5 times lower than the value of Hodge and co-workers) on both the measurements leads to an uncertainty of ±7cm^3, which is not negligible compared with the net difference.

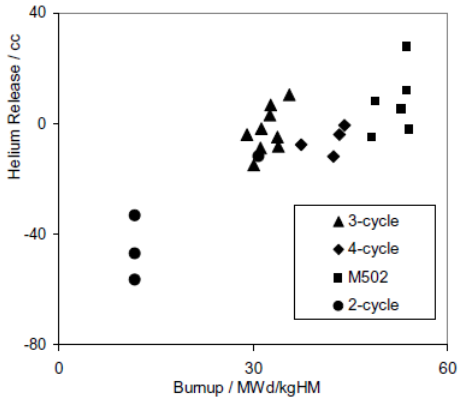

Figure 2.4 Helium release from SBR MOX fuel irradiated in the PWR reactor Beznau-1. The graph is taken from Barker et al. (2006).

2.2 Model development

An approach of intermediate complexity has been considered for the treatment of the helium release. In fact, as discussed in the previous section, simple correlations coupling the helium release to the fission gas release are applicable only in un-pressurized rods, and can fail since they are over-simplified. On the other hand, detailed reaction rate equations can be hardly developed because of the uncertainty of all the model parameters and the scarcity of experimental data in the open literature.

A simple model has been developed that takes separately into account the intra- and inter-granular behaviour and that is consistent with the current model for fission gas release in the TRANSURANUS code. Furthermore, the absorption mechanism has been included in a simplified and preliminary way.

2.2.1 Intra-granular behaviour

The main assumption of the intra-granular module is the treatment of the trapping and resolution in equilibrium (i.e., adopting an effective diffusion coefficient) and the grain boundary as a perfect sink (i.e., same assumptions of Federici et al. (2007) and TRANSURANUS fission gas release model).

The intra-granular behaviour is then modelled by a diffusion equation inside a spherical grain with a homogeneous Dirichlet boundary condition and considering an effective diffusion coefficient (D_{eff}, m^2/s).

$$\frac{\partial C_{He}}{\partial t_s} = D_{eff}\left(\frac{\partial^2 C_{He}}{\partial r^2} + \frac{2}{r}\frac{\partial C_{He}}{\partial r}\right) + He \qquad (2.8)$$

$$C_{He}(t_s, r = a) = 0$$

where r is the radial coordinate, C_{He} (mol/m^3), the concentration of helium inside the grain, He (mol/m^{3}s) the helium production rate and t_s (s) the time.

The model has been implemented in TRANSURANUS, where the diffusion equation is solved numerically by the URGAS algorithm (Elton and Lassmann, 1987; Lassmann and Benk, 2000), for each radial point. The helium production rate is computed by the model presented in the first chapter. The equivalent radius of the grain changes in time due to the grain growth, which is modelled by means of the correlation reported in reported in the previous section.

Three different diffusion coefficients ($D_{He,min}$, $D_{He,average}$ and $D_{He,max}$ - m^2/s) have been implemented in the TRANSURANUS code, based on thermal diffusion coefficients available in literature:

$$\begin{aligned} D_{He,\min} &= 8.887 \cdot 10^{-14} \cdot \exp(-17505.9/T) \\ D_{He,average} &= 1.405 \cdot 10^{-12} \cdot \exp(-17505.9/T) \\ D_{He,\max} &= 8.000 \cdot 10^{-7} \cdot \exp(-23163.5/T) \end{aligned} \qquad (2.9)$$

The first two are the lower limit and the average value of the diffusion coefficients of (Bostrom, 1958; Rufeh et al., 1965; Sung, 1967; Guilbert et al., 2004; Roudil et al., 2004; Blanpain et al., 2006), while the third one is the coefficient proposed by Ronchi and Hiernaut (2004). However, the last one is an atomic diffusion coefficient derived from the interpretation of the experimental data by means of a more complex model, which takes into account trapping and resolution separately. Furthermore it is representative of a ^{238}Pu MOX doped fuel, where the α self-irradiation is expected to have a role in the enhancement of the diffusion coefficient. For these reasons it should be used only as a conservative test case.

2.2.2 Inter-granular behaviour

The treatment of the inter-granular behaviour is based on the experimental evidence that the diffusivity of helium at the grain boundary is accelerated if temperatures are above 800°C (Martin et al., 2010). The grain boundary behaviour is then taken into account in the following way: (i) when the threshold for the fission gas release is not yet reached[3], helium is trapped in gas bubbles (mainly composed by fission gases) if temperatures are lower than 800°C, and is instantaneously released in the free volume, if temperatures are higher; (ii) if the threshold for the fission gas release is exceeded, all the helium reaching the grain boundary is instantaneously released.

[3] Once the fission gases reach the grain boundary, they are not immediately released to the free volume, but they are trapped in bubbles that grow continuously. Once the bubbles are large enough, they start to interconnect, forming tunnels, from which the gas atoms are vented out. It is then clear that fission gas release occurs only after a certain threshold, due to the bubble interconnection.

2.2.3Absorption

On the basis of the work of (Federici et al., 2007), a model has been set up, assuming that helium can infuse if the helium partial pressure in the inter-granular cavities is lower than the free volume helium partial pressure, and that these cavities are already partially filled with the helium trapped at the grain boundaries. Based on the evidence that the saturation is reached after one irradiation cycle (Federici et al., 2007), we assumed that the infusion process has a time constant of 1 MWd/kgHM (i.e., reaching the saturation after 5 MWd/kgHM). The following equation is solved:

$$\frac{bu_{sat}}{5}\frac{dn_{\inf}}{dbu} = n_{eq} - n_{GB} - n_{\inf} \tag{2.10}$$

where n_{inf} are the infused moles, bu_{sat} =5MWd/kgHM is five times the time constant, n_{eq} the number of moles in the inter-granular cavities in equilibrium with the free volume helium partial pressure, and n_{GB} is the number of moles created in the fuel and trapped at the grain boundaries.

The number of moles in equilibrium with the helium partial pressure is computed by means of the ideal gas law:

$$n_{eq} = \frac{p_{FV} \cdot \frac{n_{He.FV}}{n_{TOT.FV}} \cdot V_{He}}{R_{gas} T_{fuel,av}} \tag{2.11}$$

where p_{FV} (Pa) is the pressure in the fuel rod free volume, $n_{He,FV}$ are the moles of helium in the free volume, $n_{TOT,FV}$ are the total number of moles in the fuel rod free volume, V_{He} (m) is the volume available for the infused helium, R_{gas} = 8.314 (J/molK) is the gas constant and $T_{fuel,av}$ (K) the average fuel temperature.

Since the grain boundary release is treated separately, if the number of moles at the grain boundary is larger than the number of moles in equilibrium with the free volume helium partial pressure, $n_{eq} - n_{GB}$ is set at 0.

2.3 Model verification

In order to verify models describing the gas behaviour in fuels, the temperatures must be known. For this reason a complete thermo-mechanical analysis has to be performed. However, for most of the data present in section 2.1, fuel rod geometries and irradiation histories are not known. The only data that can be used are those of the ATR irradiation test, which has been already analysed in (Botazzoli, 2008), and the data of the SBR MOX M501.

2.3.1 ATR irradiation test

The ATR irradiation test (Ott and Morris, 2007) consists of nine weapon-grade MOX fuels fabricated at Los Alamos National Laboratories, irradiated in the Advanced Test Reactor at Idaho National Laboratory and analysed at Oak Ridge National Laboratories, in the context of the Fissile Material Disposition Program sponsored by the United States Department of Energy, and now included in the International Fuel Performance Experiment database (http://www.oecd-nea.org/tools/abstract/detail/nea-1774). The fuel rods reached a burn-up ranging from 20 to 50 MWd/kgHM.

For all the rods, helium production has been estimated by means of the depletion code ORIGEN, which has been modified including ternary fission yield and effective cross sections of the ATR reactor (Hodge et al., 2005). For the fuel rods reaching 50 MWd/kgHM (CAP5FP8, CAP6FP9, CAP12FP15), helium released in the gap was measured. These three fuel rods have been simulated. For the details of the input setting, see Appendix C.

It is worth noting that the helium production model of TRANSURANUS does not include effective cross sections of the ATR, hence standard LWR MOX cross sections have been used. However, a reasonable agreement has been found between TUBRNP and ORIGEN predictions, with differences smaller than 10%.

The computed fractional releases are shown in Figure 2.5, Figure 2.6 and Figure 2.7 by using the different diffusion coefficients, and compared with the experimental data.

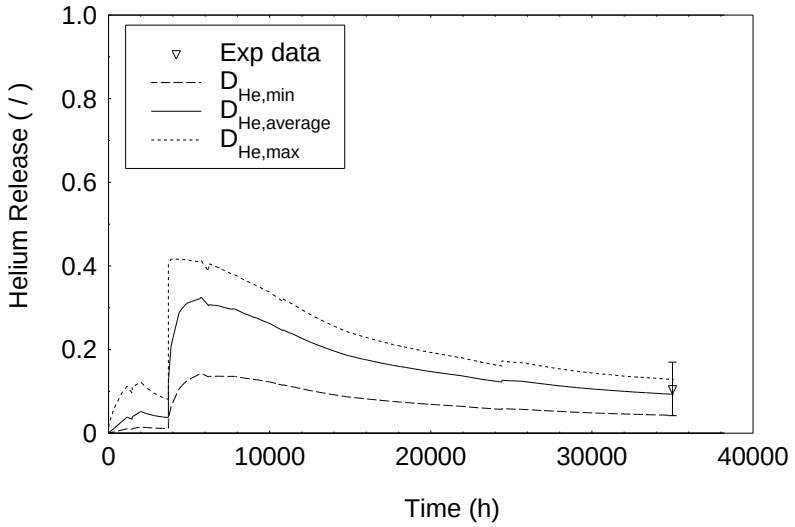

Figure 2.5 Comparison between measured and computed helium release in CAP5FP8.

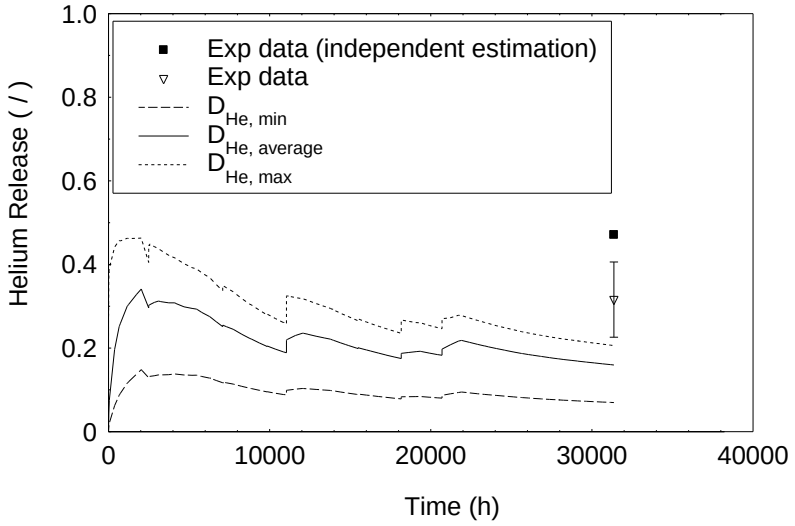

Figure 2.6 Comparison between measured and computed helium release in CAP6FP9. The "independent estimation" is the value calculated by considering the measured inner pressure, rod free volume, fraction of helium moles in the gap and produced helium.

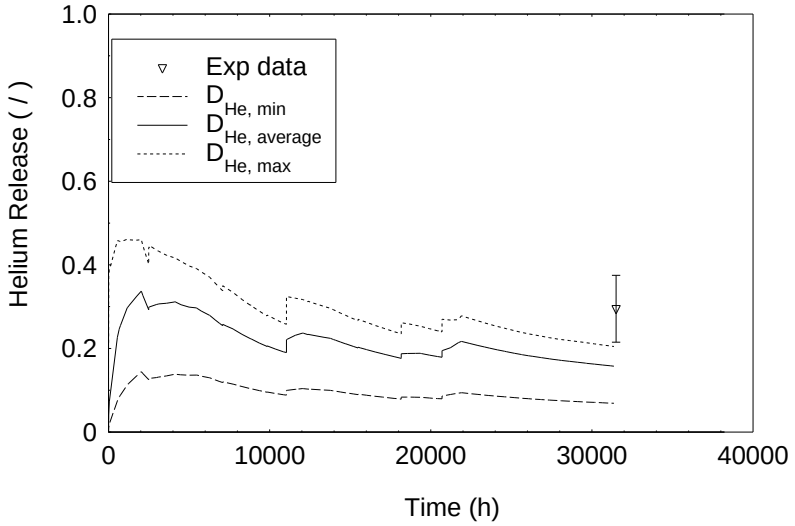

Figure 2.7 Comparison between measured and computed helium release in CAP12FP15.

Before commenting the results, it is worth mentioning that the helium fractional release of the fuel pin CAP6FP9 reported in the report of the irradiation test (Hodge et al., 2005, from now on ATR report) is not consistent with the values of other measured quantities. In fact, the fractional release is 31.6±9%, while a value of 47.1% can be calculated by

considering the measured inner pressure, rod free volume, fraction of helium moles in the gap and produced helium.

Helium release is well predicted with all the diffusion coefficients for the fuel rod CAP5FP8, while it is underestimated for the fuel pins CAP6FP9 and CAP12FP15.

However, the fission gas release is strongly underestimated. Measured fission gas release fractions are 3.37, 7.49 and 9.23%, while the present simulations lead to 0.97, 1.12 and 1.21% for CAP5FP8, CAP6FP9 and CAP12FP15, respectively. It is possible to see that for the CAP5FP8, where the fission gas release underestimation is less important, the helium release is well predicted, while for the other two fuel rods the under-prediction of helium release is important. The underestimation of fission gas release can be due to the Pu heterogeneity effect (Billaux and van Vliet, 1986; Ishida and Korei; 1994; Koo et al., 2001), which is not considered in the present simulations, or to an underestimation of the fuel temperature, which can be due to several reasons (e.g., underestimation of fuel thermal conductivity, overestimation of gap size). However, fuel temperature and fission gas release are strongly coupled, since (i) the release of fission gases decreases the thermal conductance of the gap, increasing the fuel temperature, and (ii) the increase of the fuel temperature affects the diffusion coefficient of fission gases, enhancing the release. This means that, if fission gas release is underestimated because of the Pu heterogeneity, lower temperatures are also computed, increasing the underestimation of fission gas release. As far as the helium is concerned, if lower temperatures are evaluated, less helium is predicted at the grain boundary, being available for the release. Furthermore, if the amount of fission gases at the grain boundary (in the areas of the pellet with a temperature lower than 800°C) is incorrectly predicted to be below the release threshold, also the amount of helium release from the grain boundaries of those areas is incorrectly underpredicted.

2.3.2 SBR M501-M504 Beznau-1 base irradiation

In 1994 BNFL supplied four assemblies of SBR MOX to the Swiss utility, NOK. The fuel was in a Westinghouse 14×14 PWR design clad in low-tin Zr-4. These assemblies, denoted M501 to M504, were irradiated in Beznau-1 for three cycles to an average burn-up of 34.5 MWd/kgHM. Seven rods were extracted from assembly M501 in 1998, and sent for a comprehensive post irradiation examination (PIE) programme at the JRC/ITU. The three remaining assemblies, M502 – M504, were irradiated for a further 16 months. In 2001, four rods, with burn-ups in the range 37 to 44 MWd/kgHM, were removed from assembly M504 for post irradiation examinations. In July 2001, assembly M502 was re-loaded into the reactor in a central position and irradiated for a further year to an average burn-up of about 49 MWd/kgHM (Barker et al., 2006).

Power histories and geometries of the fuel rods of the M501 have been considered. Two additional irradiation cycles with a linear power of 17 kW/m have been added, reaching a burn-up of 50 MWd/kgHM, in order to have a qualitative comparison with the fuel

rods of the assemblies M504. More Details about the TRANSURANUS input setting is given in Appendix C.

The initial porosity of the pellets was about 4.3%, with a negligible fraction of open porosities, and was supposed to decrease to 3% after the densification process. However, the total amount of helium infused at the equilibrium would reach a value much higher than the experimental evidence if we would consider that the volume available for the helium was 3% of the fuel volume. The comparisons between the model prediction and the experimental data are shown in Figure 2.8 and Figure 2.9, adopting different assumptions.

In Figure 2.8, the model neglecting the infusion (black lines) is compared with the model including the infusion (grey lines) and considering a volume of inter-granular cavities of 3% of the total fuel volume. This represents the total porosity volume after the densification. Dashed and full curves are simulations performed using the average and the maximum diffusion coefficients. It is possible to see that adopting a value of 3% for the porosity leads in any case to an overestimation of the helium infused.

In Figure 2.9, the dashed line represents the simulation adopting the average diffusion coefficient and a volume available for the helium of 1.5% of the fuel volume, while the full line represents the simulation adopting the maximum diffusion coefficient and a volume available for the helium of 1% of the fuel volume.

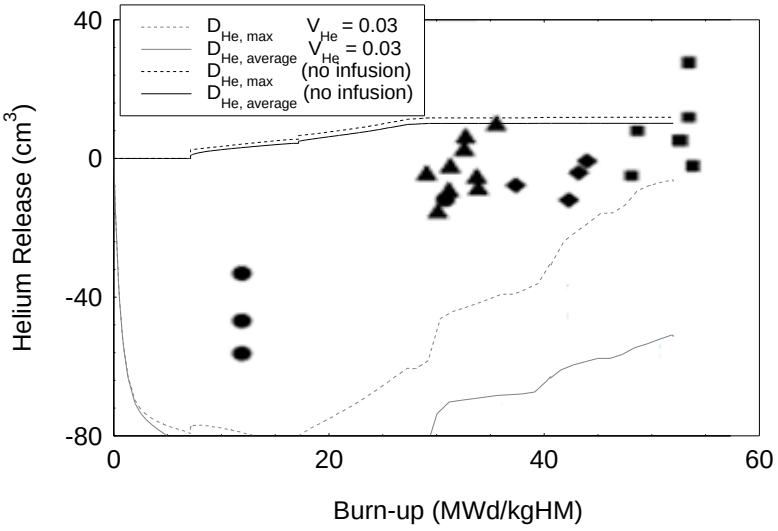

Figure 2.8 Comparison between measured and computed helium release, extreme cases.

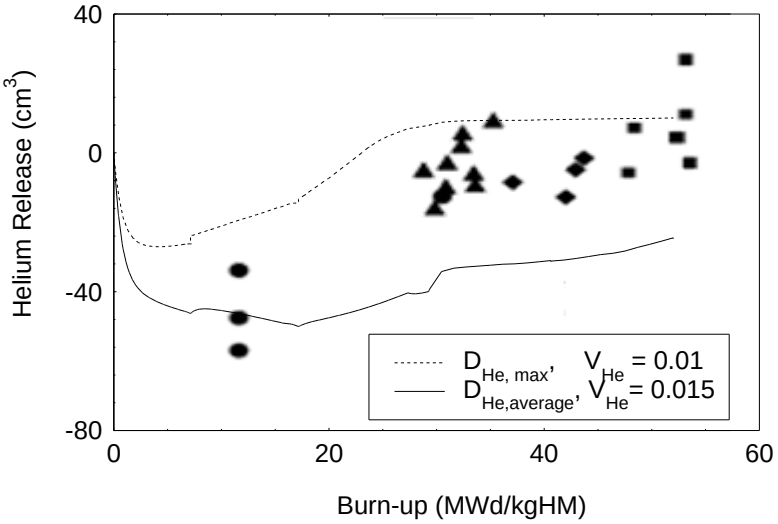

Figure 2.9 Comparison between measured and computed helium release.

It is possible to conclude that the selection of the model parameters has a great influence on the results, and, when adopting a volume fraction of 1-1.5%, the proposed model shows a reasonable agreement with the experiments. Infusion is the dominant process for low and intermediate burn-ups in pressurized rods, hence the total amount of gas in equilibrium in the fuel is the most important "parameter" under these conditions. Nevertheless, also the intra-granular diffusion coefficient is of relevance. In fact, it affects the time needed for a net release of helium. However, a better insight and more experimental data are required to better assess the helium infusion/release process.

2.4 Concluding remarks

The helium release is frequently neglected or considered as an empirical function of the fission gas release in fuel performance analysis. A model was not present in TRANSURANUS, but a constant fraction (defined by the user) of the produced helium was considered as released. In this chapter, a first model for the release of helium in oxide fuels has been proposed and implemented. In a simple and physical way, it takes into account the intra- and inter-granular behaviour (by solving the diffusion on the grain and the release from the grain boundary), and the absorption. The parameters have been evaluated on the basis of information found in the open literature. The model has been implemented in the TRANSURANUS code, coupled with the helium production and grain growth models, and preliminarily validated on the basis of the ATR irradiation test and of the SBR M501-M504 fuel assemblies base irradiated in the PWR reactor Beznau-1. The analysis of the ATR showed some discrepancies. However, the

underestimation in the helium release for two of the simulated rods can be caused by the underestimation of the fission gas release, which in turn can be caused by errors in the temperature calculation. As far as the SBR M501-M504 irradiation is concerned, the selection of the model parameters largely influences the results. The adoption of a volume fraction of inter-granular porosity equal to 3% (in accordance with the porosity after the densification process) leads to an overestimation of the helium infused. Reducing this value to 1-1.5% brings to a reasonable agreement with the experiments. However, a better insight and more experimental data are required to better assess the helium infusion process.

(This page has been intentionally left blank)

Conclusions

The present work contributes to the study and the modelling of the helium behaviour (from its production to the release) in oxide nuclear fuels for LWRs. Helium behaviour can influence the fuel performance, hence the design, licensing and operation of a fuel rod. In addition, it affects the long term storage of nuclear fuel. During the irradiation, helium trapped in the pellet can contribute to the degradation of the properties of the fuel. However, the extent of this influence is still an open issue. On the other hand, the fraction released in the gap between the fuel and the cladding influences the rod inner pressure with important consequences for the safety. This is especially relevant in case of the lifetime extension of MOX fuels. In fact, as shown in the first chapter, helium production increases exponentially with the burn-up and it is more relevant for MOX fuel, since the initial presence of plutonium leads to a larger production of the main α emitters. To this end, models relevant for the performance of LWR UO_2 and MOX fuels at high burn-ups have been developed, coupled and implemented in the TRANSURANUS code.

In particular, a model for the production of helium in LWR oxide fuels has been developed and implemented in TUBRNP. The model takes into account the helium produced by alpha decays, (n,α) reactions and ternary fissions. At first, it has been verified by means of detailed neutron-transport depletion calculations, performed by means of the VESTA Monte Carlo-depletion code. A good agreement has been found in terms of helium produced and actinides concentrations for both the UO_2 and MOX cases. Finally, the model has been validated against limited experimental data available in the open literature. In particular, a good agreement has been found in terms of average concentrations and radial profiles of the main α emitters produced in UO_2 fuels. However, further experimental data are needed for a more exhaustive validation of the model. The most important missing information is the helium produced. Moreover, isotopic compositions and relative radial nuclide profiles of LWR MOX fuels, especially at high burn-up, are also important.

As a final step, the transport of helium in the fuel has been investigated. A model for the release of helium in the gap between the fuel and the cladding has been developed,

implemented in TRANSURANUS and preliminarily validated on the basis of pressurized and unpressurized fuel rods. The agreement is satisfactory, although some discrepancies have been noticed. More experimental data are needed for a better assessment of the model parameters (diffusion coefficients, solubilities) and for a proper validation of the model.

In summary, the behaviour of helium in LWR fuel has been studied and modelled, considering the production, the release in the fuel rod free volume and the absorption. Some data would be useful for a complete validation of the helium production and release models of LWR MOX fuels. Although related to LWR conditions, the present work could be extended to fast reactors. This could be achieved by including specific one-group cross sections in the helium production model, by considering the columnar grain growth and the relative release process from columnar grains.

Nomenclature

Latin symbols

a (m)	radius of the equivalent booth sphere
$A(r)$	conversion factor TUBRNP
$BR_{Am241(n,\gamma)\,Am242m}$	branching ratio for the ^{241}Am(n,γ) ^{242m}Am reaction
bu (MWd/kgHM)	burn-up
bu_{sat} (MWd/kgHM)	five time the time constant for the helium absorption
C	generic normalization constant
C_{He} (moli/m^3)	concentration of helium inside the grain
$dbu(r)$ (MWd/kgHM)	local burn-up increment
D_{eff} (m^2/s)	effective diffusion coefficient taking into account trapping and resolution
$D_{eff,GB}$ (m^2/s)	grain boundary effective diffusion coefficient
$D_{He,average}$ (m^2/s)	average helium diffusion coefficient
$D_{He,max}$ (m^2/s)	helium diffusion coefficient by Ronchi and Hiernaut
$D_{He,max,\,NoR}$ (m^2/s)	maximum diffusion coefficient of helium excluding Ronchi and Hiernaut
$D_{He,min}$ (m^2/s)	minimum helium diffusion coefficient
dt (h)	time step
E (eV)	energy of the incident neutron
E_{fiss} (MWd)	energy released per fission

f	generic function
$f_m(r)$	form factor that reflects the radial dependence of absorption of epi-thermal or resonance neutrons of the nuclide m
g_{rel}	amount of gas released
g_{sol}	amount of gas in solution
g_{trap}	amount of gas trapped
He (mol/m^{3}s)	helium production rate
H_{RH}	gas de-trapping rate
k_B	Boltzmann constant
K_{RH}	gas trapping rate
n_{eq}	number of moles in the inter-granular cavities in equilibrium with the free volume helium partial pressure
$n_{fiss}(r)$ (fissions/cm^3)	density of fissions
n_{GB}	number of moles created in the fuel and trapped at the grain boundaries
$n_{He,FV}$	moles of helium in the free volume
n_{inf}	number of infused moles
$N_m(r)$ (at/cm^3)	local concentration of the nuclide m (r = radial coordinate)
$n_{TOT,FV}$	total number of moles in the fuel rod free volume
p_1	empirical constant of the form factor $f_m(r)$
p_2	empirical constant of the form factor $f_m(r)$
p_3	empirical constant of the form factor $f_m(r)$
p_{FV} (Pa)	pressure in the fuel rod free volume
$q'''(r)$ (MW/cm^3)	local power density
r	radial coordinate
R_{fuel} (cm)	fuel outer radius
R_{gas} (J/(molK))	gas constant

S_{RH}	gas de-sorption rate
t (h)	time
T (K)	temperature
$T_{fuel,av}$ (K)	average fuel temperature
t_s (s)	time in seconds
U_{RH}	release rate of the amount of gas trapped
V_{He} (m^3)	volume available for the infused helium
y_{He}	fission yield for the production of helium

Greek symbols

λ (h^{-1})	decay constants
ρ_{HM} (kgHM/cm^3)	density of heavy metals
$\sigma(E)$ (barn)	cross section
$\sigma_{a,m}$ (barn)	one-group effective cross sections for total neutron absorption
$\sigma_{a,O16}$ (barn)	^{16}O one-group total absorption effective cross section
$\sigma_{Am241(n,\gamma)}(E)$ (barn)	cross section for the reaction (n,γ) on ^{241}Am, independent of the product
$\sigma_{Am241(n,\gamma)Am242m}(E)$	cross section for the reaction ^{241}Am(n,γ)^{242m}Am expressed in (barn)
$\sigma_{c,m}$ (barn)	one-group effective cross sections for total neutron capture
$\sigma_{fiss,i}$ (barn)	one-group fission cross section of the i-th nuclide
$\sigma_{\alpha,O-16}$ (barn)	one-group effective ^{16}O(n,α)^{13}C cross section
τ	equivalent dimensionless time for the intra-granular diffusion
τ_{GB}	equivalent dimensionless time for the grain boundary diffusion
Φ (n/(barn·h))	total neutron flux
$\Phi \cdot dt$ (n/barn)	neutron fluence
$\Psi(E)$ (1/eV)	neutron spectrum

(This page has been intentionally left blank)

References

Aybar, H. S., Ortego, P. (2005). A Review of Nuclear Fuel Performance Codes, *Progr Nucl Energ*, vol. 46, No. 2, pp. 127-141.

Barker, M.A., Matthews, E.C., Stephenson, K., Brémier, S., Papaioannou, D., Walker**,** C.T., Parmar, Y. (2006). Post-irradiation examination of high burnup sbr mox fuel, *Transactions of Topfuel 2006*, pp. 5-9, Salamanca, Spain, October, 22-26, 2006.

Bart, G., Gebhardt, O., Aerne, E. T., Martin, M. (1994). *Proceedings of IAEA Technical Committee Meeting on Development of Post-Irradiation Examination at the Reactor Fuel Examination Facility*, Cadarache, France, 1994, IAEA-TECDOC-822, 1995, p. 337.

Billaux, M., van Vliet, J. (1986). Impact of Fuel Heterogeneities on Fission Gas Release for LWR U-Pu mixed oxide fuels, *Res Mechanica* 17.

Blanpain, P., Lippens, M., Schut, H. V., Federov, A., Bakker, K. (2006). The HARLEM Project. *Materials Models and Simulations for Nuclear Fuels (MMSNF-5).* June 1-2, Nice, France.

Booth, A. H. (1957) A suggested method for calculating the diffusion of radioactive rare gas fission products from UO_2 elements and a discussion of proposed in-reactor experiments that may be used to test its validity, Report DCI-27, AECL, Chalk River, Ontario, Canada.

Bostrom, W. A. (1958) In J. Belle's Paper. Properties of Uranium Dioxide, *Proc. of the Second United Nations International Conference on Peaceful Uses of Atomic Energy*, Geneva, 6, 569-589.

Botazzoli, P. (2008). Verification of the Fission Gas Release Predictions of the TRANSURANUS Code for LWR MOX Fuel, Technical Note, JRC-ITU-TN-2008/20, © European Communities.

Bowden R. L., Thorne, P. R. (2002). Problem Specification for the OECD/NEANSC Burnup Credit Benchmark Phase IV-A: Mixed Oxide (MOX) Fuels, Technical Report, British Nuclear Fuel.

Bowman, S. M. (2007). Overview of the Scale Code System, *American Nuclear Society 2007 Winter Meeting "Making the Renaissance Real"*, November 11–15, 2007. Washington, DC.

Bowman, S. M., Leal, L. C., Hermann, O. W., Parks, C. V. (1999). Origen-Arp, A Fast And Easy-To-Use Source Term Generation Tool, *Ninth International Conference on Radiation Shielding Half a Century of Radiation Shielding Research and its Evolution into the Next Era (ICRS-9)*, October 17–22, 1999, Tsukuba, Japan.

Briesmeister, J. F., (2000). MCNP - A General Monte CarloN-Particle Transport Code", Version 4C. LA-13709-M. Los Alamos, NM, Los Alamos National Laboratory.

Cacuci, D. G. Editor (2010). Handbook of Nuclear Engineering, Vol. 2, Chap. 12, and Vol. 3, Chap. 13, Springer.

Chadwick, M. B., Oblozinsky, P., Herman, M., Greene, N. M., McKnight, R. D., Smith, D. L., Young, P. G., MacFarlane, R. E., Hale, G. M., Haight, R. C., Frankle, S., Kahler, A. C., Kawano, T., Little, R. C., Madland, D. G., Moller, P., Mosteller, R., Page, P., Talou, P., Trellue, H., White, M., Wilson, W. B., Arcilla, R., Dunford, C. L., Mughabghab, S. F., Pritychenko, B., Rochman, D., Sonzogni, A. A., Lubitz, C., Trumbull, T. H., Weinman, J., Brown, D., Cullen, D. E., Heinrichs, D., McNabb, D., Derrien, H.,, Dunn, M., Larson, N. M., Leal, L. C., Carlson, A. D., Block, R. C., Briggs, B., Cheng, E., Huria, H., Kozier, K., Courcelle, A., Pronyaev, V., van der Marck, S. C., (2006). Evaluated Nuclear Data file ENDF/B-VII.0. *Nucl Data Sheets*, 107, 12, 2931–3118.

Cousin, L., Haeck, W., Cochet, B. (2010). Validating the VESTA Monte Carlo Depletion Interface using ARIANE Chemical Assay Data for Pressurized Water Reactor Applications, *Proceedings of International Conference on the Physics of Reactors (PHYSOR),* Pittsburgh, Pennsylvania, USA, 2010.

Croff, A. G., (1980). A User's Manual for the ORIGEN2 Computer Code, Technical Report ORNL/TM-7175, Oak Ridge, TN, Oak Ridge National Laboratory.

Desgranges, L., Pasquet, B., Valot, C., Roure, I. (2006a). SIMS characterisation of actinide isotopes in irradiated nuclear fuel, *J Nucl Mater* 385, 99.

Desgranges, L., Valot, C., Pasquet, B. (2006b). Characterisation of Irradiated Nuclear Fuel with SIMS, *Appl Surf Sci* 252, 7048.

Duderstadt, J. J., Hamilton, L. J. (1976). Nuclear reactor analysis, Ed. John Wiley & sons.

Elton, P. T., Lassmann, K. (1987). Calculational methods for diffusional gas, *J Nucl Mater* 101, 259-265.

Federici, E., Courcelle, A., Blanpain, P., Cognon, H. (2007). Helium production and behaviour in nuclear oxide fuels during irradiation in LWR. *Proceedings of the 2007 International LWR Fuel Performance Meeting*, September 30 – October 3, 2007, San Francisco, California.

Forrest, R. A., Kopecky, J., Sublet, J.- Ch., (2007). The European Activation File: EAF-2007 neutron-induced cross section library, Technical Report EASY Documentation Series UKAEA FUS 535, EURATOM/UKAEA Fusion Association, Abingdon, United Kingdom.

Guilbert, S., Sauvage, T., Garcia P., et al. (2004). Helium Migration in Implanted UO_2 Sintered Disks, *J Nucl Mater* 327, 88-96.

Haeck, W. (2009). VESTA User's Manual - Version 2.0.0, IRSN Report DSU/SEC/T-2008-331.

Hodge, S. A., Morris, R. N., Ott, L. J. (2005). Weapons-derived Mixed Oxide fuel test irradiation summary, Report ORNL/TM-2005/255, Oak Ridge National Laboratory, Oak Ridge, Tennessee.

Ishida, M., Korei, Y. (1994). Modelling and parametric studies of the effect of Pu-mixing heterogeneity on fission gas release from mixed oxide fuels of LWRs and FBRs, *J Nucl Mater* 210.

Kamimura, K., Kobayashi, Y., Nomata, T. (1999). Helium generation and release in MOX Fuels, *Proceedings of the symposium on MOX Fuel Cycle Technologies for Medium and Long Term Deployment*, IAEA-SM-358/19, Vienna, Austria, 17–21 May 1999.

Katsuyama, K., Ishimi, A., Maeda, K., Nagamine, T., Asaga, T. (2010). Helium release from the uranium–plutonium mixed oxide (MOX) fuel irradiated to high burn-up in a fast breeder reactor (FBR), *J Nucl Mater* 401, Issues1-3, 86–90.

Killeen, J., Sartori, E., McGrath, M. (2009). FUMEX-III: A New IAEA Coordinated Research Project on Fuel Modelling at Extended Burnup, *Proceedings of Top Fuel 2009*, Paper 2176, pp. 336-343, Paris, France, September 6-10, 2009.

Killeen, J., Turnbull, J. A., Sartori, E. (2007). Fuel Modelling at Extended Burnup: IAEA Coordinated Research Project FUMEX-II, *Proceedings of International LWR Fuel Performance Meeting*, American Nuclear Society, San Francisco, California, USA, 2007, p. 261.

Kochunas, B. M. (2008). Advanced Simulations of Heterogeneous Light Water Reactor Cores for Transuranic Recycle, Master Thesis, University of California, Berkeley.

Koo, Y., Lee, B., Cheon, J., Sohn, D. (2001). Modeling and parametric studies of the effect of inhomogeneity on fission gas release in LWR MOX fuel, *Ann Nucl Energy* 13.

Kryukov, F. N., Lyadov, G. D., Nikitin, O. N., Smirnov, V. P., Chetverikov, A. P. (2006). Radial distribution of the burn-up and content of Plutonium in VVER fuel pellets (translated from Russian), *Atom Energy+* 100, 1.

Kurita, I., Kikuchi, K., Abe, T. (1999). MOX Fuel Irradiation Behaviour in a Thermal Reactor, *Proceedings of the symposium on MOX Fuel Cycle Technologies for Medium and Long Term Deployment*, IAEA-SM-358/17, Vienna, Austria, 17–21 May 1999.

Lassmann, K. (1992). TRANSURANUS: A fuel rod analysis code ready for use, *J Nucl Mater*, 188, 295–302.

Lassmann, K., Benk, H. (2000). Numerical algorithms for intragranular fission gas release, *J Nucl Mater* 280, 127-135.

Lassmann, K., O'Carroll, C., van de Laar, J., Walker, C. T. (1994). The radial distribution of Plutonium in high burn-up UO_2 fuels, *J Nucl Mater*, 208, 223–231.

Lassmann, K., Walker, C. T., van de Laar, J. (1998). Extension of the TRANSURANUS burnup model to heavy water reactor conditions , *J Nucl Mater*, 255, Issues 2-3, 222-233.

Lombardi, C. (2004). Impianti Nucleari, Ed. Cusl, sixth edition, Milano, Italy.

Manzel, R., Walker, C. T. (2000). High burn-up fuel microstructure and its effect on fuel rod performance, *Proceedings of Topical Meeting on LWR Fuel Performance (Oral Session)*, American Nuclear Society, Park City, Utah, USA, 2000, p. 604.

Manzel, R., Walker, C. T. (2002). EPMA and SEM of fuel samples from PWR rods with an average burn-up of around 100 MWd/kgHM, *J Nucl Mater* 301, 170.

Martin, G., Garcia, P., Sabathier, C., Carlot, G., Sauvage, T., Desgardin, P., Raepsaet, C., Khodja, H. (2010). Helium release in uranium dioxide in relation to grain boundaries and free surfaces, *Nucl Instrum Meth B* 268, 2133-2137.

Matzke, Hj. (1980). Gas release mechanisms in UO_2—A critical review**,** *Radiat Eff* 53, 219–242.

Maugeri, E., Wiss, T., Hiernaut, J. P., Desai, K., Thiriet, C., Rondinella, V. V., Colle, J. Y., Konings, R. J. M. (2009). Helium solubility and behaviour in uranium dioxide, *J Nucl Mater* 385, 461–466.

Nakahara, Y., Suyama, K., Suzaki, T. (2002). Technical Development on Burn-up Credit for LWR Spent Fuels (English Translation), JAERI-Tech 2000-071(ORNL/TR-2001/01), Oak Ridge National Laboratory, Oak Ridge, Tennessee.

OECD/NEA. (2006). *The JEFF-3.1 Nuclear Data Library – Jeff report 21.* Technical Report ISBN 92-64-02314-3, NEA databank.

Olander, D. R. (1976). Fundamental Aspects of Nuclear Reactor Fuel Elements: National Technical Information Services, P26711-P1, University of California, Berkeley, California.

ORNL (2006). SCALE: A Modular Code System for Performing Standardized Computer Analyses for Licensing Evaluations, ORNL/TM-2005/39, Version 5.1, Vols. I-III.

Ott, L. J., Morris, R. N. (2007). Irradiation tests of Mixed-Oxide Fuel prepared with Weapons-derived Plutonium, *J Nucl Mater* 371, Issues 1-3, 314-328.

Pelowitz, D. B. (2005). MCNPX User's Manual, Version 2.5.0. LA-CP-05-0369, Los Alamos, NM, Los Alamos National Laboratory.

Ronchi, C., Hiernaut, J. P. (2004). Helium diffusion in uranium and plutonium oxides, *J Nucl Mater*, vol. 325, pp. 1-12.

Roque, B. (2007). Working Party on Scientific Issues of Reactor System – Specification for the Phase 2 of a Depletion Calculation Benchmark devoted to MOx Fuel Cycles, Technical Report, NEA/NSC/DOC(2007)9.

Roudil, D., Deschanels, X., Trocellier, P., Jegou, C., Peuget, S., Bart, J. M. (2004). Helium Thermal Diffusion in a Uranium Dioxide Matrix, *J Nucl Mater* 325, 148-158.

Ruetten, H.J., (1993). The depletion computer code ORIGEN-JUEL-II, Germany. http://hdl.handle.net/10068/169525

Rufeh, F., Olander D. R., Pigford, T. H. (1965). The Solubility Of Helium In Uranium Dioxide, *Nucl Sci Eng* 23, 335-338.

Schubert, A., Van Uffelen, P., van de Laar, J., Walker, C. T., Haeck, W. (2008). Extension of the TRANSURANUS burn-up model. *J Nucl Mater* 376 (1), 1-10.

Shibata, K., Iwamoto, O., Nakagawa, T., Iwamoto, N., Ichihara, A., Kunieda, S., Chiba, S., Furutaka, K., Otuka, N., Ohsawa, T., Murata, T., Matsunobu, H., Zukeran, A., Kamada, S., Katakura, J., (2011). JENDL-4.0: A New Library for Nuclear Science and Engineering (to be published to *J Nucl Sci Technol*).

Shibata, K., Iwamoto, O., Nakagawa, T., Iwamoto, N., Ichihara, A., Kunieda, S., Chiba, S., Otuka, N, Katakura, J. (2010). JENDL-4.0: A New Library for Innovative Nuclear Energy Systems, *Proceedings of the International Conference on Nuclear Data for Science and Technology (ND2010)*, April 26–30, 2010, Jeju Island, Korea.

Sontheimer, F., Landskron, H. (2000). Puzzling features of EPMA radial fission gas release profiles: The key to realistic modeling of fission gas release up to ultra-high burn-up of 100 MWd/kgM with CARO-E, V. Onoufriev (Ed.), *Proceedings of IAEA Technical Committee Meeting on Nuclear Fuel Behaviour Modelling at High Burnup*, Lake Windermere, UK, 2000, IAEA-TECDOC-1233, 2001, p. 105.

Speight, M. V. (1969). A calculation on the migration of fission gas in material exhibiting precipitation and resolution of gas atoms under irradiation, *Nucl Sci Eng* 37.

Sung, P. (1967). Equilibrium Solubility and Diffusivity of Helium in Single-Crystal Uranium Oxide, Ph.D. Thesis, University of Washington.

Taguchi, G., Konishi, S. (1987). Taguchi methods: orthogonal arrays and linear graphs, ASI Press, Dearborn, USA.

TRANSURANUS - Lassmann, K., Shubert, A., Van Uffelen, P., Gyori, Cs., van de Laar, J. (2009). TRANSURANUS Handbook, Copyright ©1975-2009, ITU (Institute for Transuranium Elements), Karlsruhe.

Van Uffelen, P. (2006). Modelling of Nuclear Fuel Behaviour, EUR 2231 EN, Institute for Transuranium Elements.

Walker, C. T. (1999). Electron probe microanalysis of irradiated nuclear fuel: an overview, *J Anal Atom Spectrom* 14, 447.

Walker, C. T., Bremier, S., Portier, S., Hasnaoui, R., Goll, W. (2009). SIMS analysis of an UO_2 fuel irradiated at low temperature to 65 MWd/kgHM, *J Nucl Mater* 393, 212-223.

(This page has been intentionally left blank)

Appendix A
MCNP Simulations

In the present appendix, some details about the performed MCNP Monte Carlo simulations are given. These simulations have been carried out in order to compute typical neutron spectra of PWR and BWR reactors, loaded with different oxide fuels (i.e., UO_2 with different enrichments and MOX with different compositions). The computed spectra have been used for the evaluation of effective one-group cross sections. In the following the main modelling assumptions are reported. The cross section library JEFF 3.1 has been adopted.

Geometry: to simulate the conditions of a typical PWR (BWR), a cell with reflective boundary conditions, containing water and a pin with a fuel diameter of 8.2 mm (10.4 mm), a cladding outer diameter of 9.4 mm (12 mm) and a pin pitch of 12.55 mm (16.1 mm) has been considered (see Figure A.1). Geometrical data have been taken from Duderstadt and Hamilton (1976).

Moderator: water with a density of 725 kg/m^3 has been considered for the PWR. This value corresponds to the conditions of 15.5 MPa and 300°C. As far as the BWR is concerned, the water density should be a function of the fuel rod height. By considering typical BWR thermo-hydraulic parameters, i.e. coolant pressure of about 7 MPa, inlet temperature of 270-275°C and outlet vapour quality of 10-15%, it is possible to find a coolant density ranging from 800 to 180 kg/m^3. For this reason, different simulations have been performed with different water densities.

Cladding: Zircaloy-4 cladding has been considered for the PWR simulations and Zircaloy-2 for the BWR ones.

Fuel: UO_2 fuels with an enrichment from 2% to 5%, and different MOX compositions with plutonium content from 3% to 8% have been considered. In Table A.1 the detailed compositions are reported, MOXTU1 and MOXTU2 are the two standard compositions of the TUBRNP cross section dataset, while the others are taken from the open literature (Bowden and Thome, 2002; Roque, 2007).

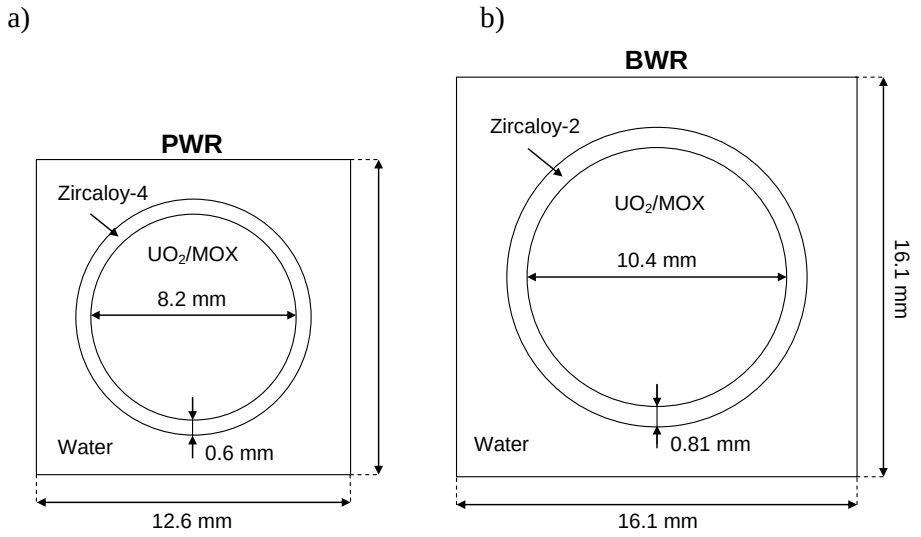

Figure A.1 Simulated cells: a) PWR and b) BWR.

Table A.1 Different MOX compositions.

Isotope	**Concentrations (at/(cm·barn))**					
	MOX1*	MOX2**	MOX3**	MOX4**	MOXTU1***	MOXTU2***
^{234}U	$4.27\cdot10^{-7}$	$2.80\cdot10^{-7}$	$2.85\cdot10^{-7}$	$2.73\cdot10^{-7}$	-	-
^{235}U	$4.83\cdot10^{-5}$	$5.86\cdot10^{-5}$	$5.95\cdot10^{-5}$	$5.71\cdot10^{-5}$	$7.13\cdot10^{-5}$	$6.98\cdot10^{-5}$
^{236}U	$8.54\cdot10^{-7}$	-	-	-	-	-
^{238}U	$2.13\cdot10^{-2}$	$2.31\cdot10^{-2}$	$2.34\cdot10^{-2}$	$2.25\cdot10^{-2}$	$2.37\cdot10^{-2}$	$2.32\cdot10^{-2}$
^{238}Pu	$8.15\cdot10^{-6}$	$2.47\cdot10^{-5}$	$4.90\cdot10^{-7}$	$7.85\cdot10^{-5}$	$1.32\cdot10^{-5}$	$2.21\cdot10^{-5}$
^{239}Pu	$6.56\cdot10^{-4}$	$8.06\cdot10^{-4}$	$9.12\cdot10^{-4}$	$7.04\cdot10^{-4}$	$4.41\cdot10^{-4}$	$7.35\cdot10^{-4}$
^{240}Pu	$2.02\cdot10^{-4}$	$3.13\cdot10^{-4}$	$5.83\cdot10^{-5}$	$5.45\cdot10^{-4}$	$1.84\cdot10^{-4}$	$3.06\cdot10^{-4}$
^{241}Pu	$7.41\cdot10^{-5}$	$1.65\cdot10^{-4}$	$3.87\cdot10^{-6}$	$2.33\cdot10^{-4}$	$5.51\cdot10^{-5}$	$9.19\cdot10^{-5}$
^{242}Pu	$2.78\cdot10^{-5}$	$5.40\cdot10^{-5}$	$4.82\cdot10^{-7}$	$3.86\cdot10^{-4}$	$4.19\cdot10^{-5}$	$6.98\cdot10^{-5}$
^{241}Am	$1.46\cdot10^{-5}$	-	-	-	-	-
^{16}O	$4.47\cdot10^{-2}$	$4.90\cdot10^{-2}$	$4.90\cdot10^{-2}$	$4.90\cdot10^{-2}$	$4.90\cdot10^{-2}$	$4.90\cdot10^{-2}$

* Roque, 2007 **Bowden and Thome, 2002 ***Lassmann ,1992

The computed spectrum of one of the analysed cases (PWR, 3.5% enriched UO_2) is shown in Figure A.2 as an example, and it is compared with the typical trend of the three components of a LWR spectrum that can be found in literature. The thermal component refers to the typical Maxwellian distribution ($C\cdot E\cdot exp(-E/k_BT)$, C being a normalization constant, E the energy, k_B the Boltzmann's constant and T the absolute temperature, the epithermal component refers to the typical trend inversely proportional to the energy, while the ^{235}U prompt neutron fission spectrum (Watt spectrum, obtained from Lombardi, 2004) has been considered as representative of the fast contribution.

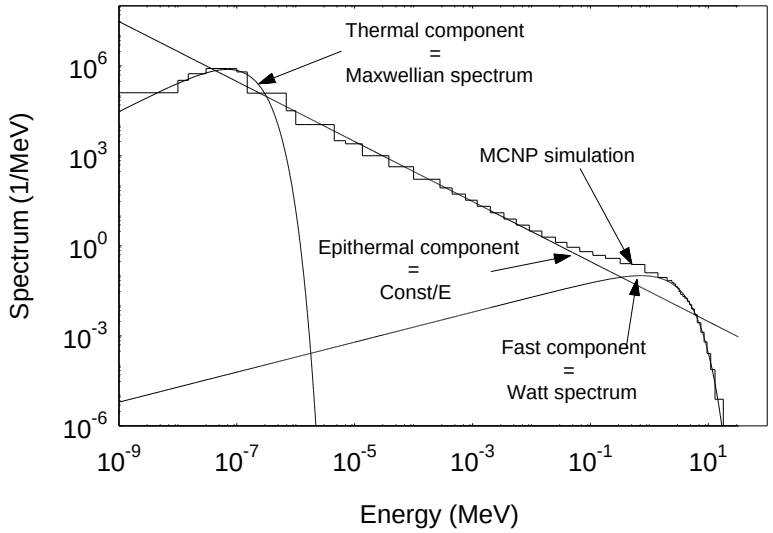

Figure A.2 Comparison between the computed spectrum and the expected trend.

(This page has been intentionally left blank)

Appendix B
Main input parameters of the simulation of the ATR MOX database with TRANSURANUS

In this appendix, the main input parameters for the simulations of the fuel rods CAP5 FP8, CAP6 FP9 and CAP12 FP15 of the ATR MOX database are given.

Power histories are given in Figures B.1, B.2 and B.3.

In Table B.1, the main geometrical parameters are summarized, while in Table B.2, the selection of the main models is given. The fuel is characterized by the following isotopic composition (at/atHM): ^{235}U = 0.0025317, ^{239}Pu = 0.0467753, ^{240}Pu = 0.0029954; ^{241}Pu = 0.00006, ^{242}Pu = 0.000011. Note that this is a weapon grade MOX.

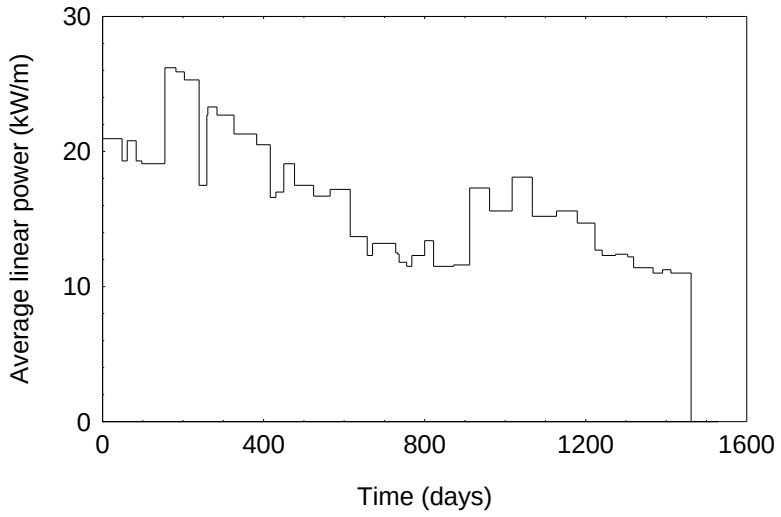

Figure B.1 Average linear power of CAP5FP8 as a function of time.

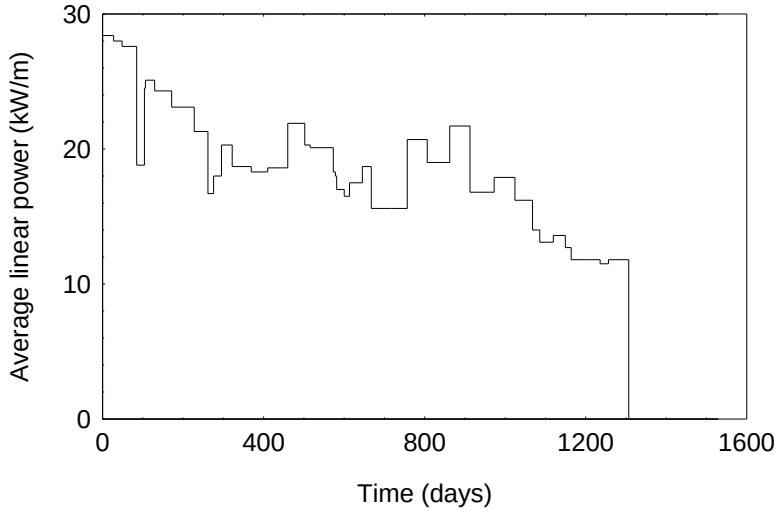

Figure B.2 Average linear power of CAP6FP9 as a function of time.

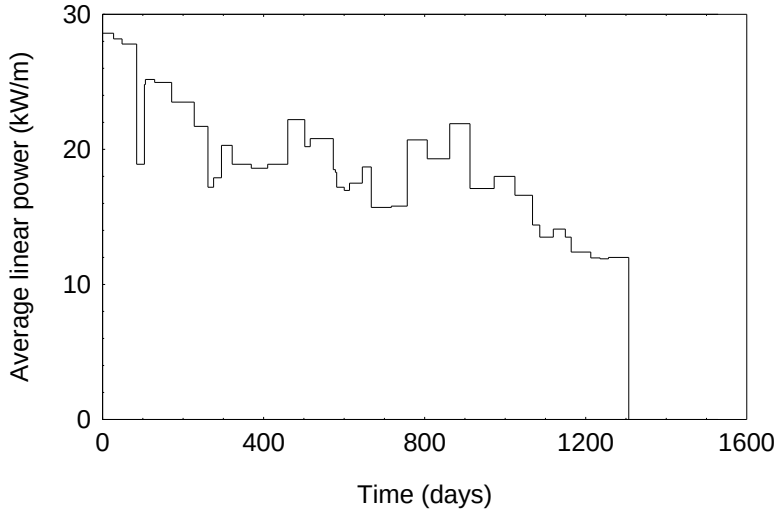

Figure B.3 Average linear power of CAP9FP12 as a function of time.

Table B.1 Main geometrical parameters.

	CAP5FP8	**CAP6FP9**	**CAP12FP15**
Outer cladding radius (mm)	4.83	4.83	4.83
Inner cladding radius (mm)	4.18	4.18	4.18
Fuel radius (mm)	4.14	4.14	4.14
Fuel stack height (mm)	147.73	148.06	147.19
Free volume (mm^3)	1318.08	1300.00	1325.96

Table B.2 Main model selection of the TRANSURANUS input files.

Variable	Value	Meaning
IKUEHL	1	Prescribed coolant temperature
IALPHA	2	Convective heat exchange coefficient of the coolant $\rightarrow \infty$
IZENKA	0	Central void formation not considered
ISTZNE	0	Restructuring not considered
IPURE	0	Pu redistribution not considered
IOXIRE	0	Oxygen redistribution not considered
INTAXL	1	Interaction between fuel and cladding is considered
IHBS	1	High burn-up structure is considered only for thermal analyses
IRELOC	8	Modified FRAPCON-3 relocation model
IDENSI	2	Simplified densification model
IDIFSOLV	0	Intra-granular FGR computed by means of URGAS algorithm
FGRMOD	6	Matzke thermal coefficient, constant athermal coefficient
IGRBDM	2	Saturation concentration at grain boundary α 1/T
MODFUEL(1:20)*	20	Standard LWR fuel properties
MODFUEL (4)	18	Fuel swelling modified FRAPCON-3 model
MODFUEL (6)	31	Best estimate MOX fuel thermal conductivity
MODCLAD(1:20)	20	Standard LWR cladding properties
RRRR1	85000 [MWd/tHM]	Threshold BU from the HBS
KORNGR	0.0102 [mm]	Fuel grain diameter
OPENPOR	1 (%)	Open porosity
IFORM	5	Local power density calculated according to the TUBRNP model
OZUM0	2	Ratio between Oxygen and Metal (O/M)
PRODIS**	0.00788/0.0103	Fraction of dish volume
POR000**	0.048/0.055	Total fabrication porosity
DENPOR**	0.029/0.0361	Porosity at the end of sintering
DENBUP	10000 (MWd/kgHM)	Burn-up at which sintering has stopped
ISLICE	1	Slice option for the axial discretisation
M3	15	Number of slices
Pi0ein	0.07652 (MPa)	Fill gas pressure at 20°C

* Except modfuel 4 and 6

** The first value refers to the pins with the treatment for gallium removal, while the second refers to the pin without the treatment

(This page has been intentionally left blank)

Appendix C
Main input parameters of the simulation of the SBR M501-M504 base irradiation with TRANSURANUS

In this appendix, the main input parameters for the simulations of the SBR M501-M504 fuel assembly base irradiation in the PWR Beznau-1 reactor are presented. In particular, only one fuel rod has been simulated, since the power histories of the other rods were similar. The power history has been extended with two additional cycles of 17kW/m in order to reach an average burn-up of about 50 MWd/kgHM. The choice of two additional cycle of 17kW/m is based on the information of the fuel assembly M504 reported in (Barker et al., 2006).

In Table C.1, the main geometrical parameters are summarized, while in Table C.2 the selection of the main models is given. The fuel is characterized by the following isotopic composition (at/atHM): ^{235}U = 0.00290, ^{238}Pu = 0.0001, ^{239}Pu = 0.02612, ^{240}Pu = 0.00964; ^{241}Pu = 0.00171, ^{242}Pu = 0.00047; ^{241}Am = 0.00015.

In Figure C.1, the average linear power of the selected rod is shown as a function of time. The fast spectrum is obtained multiplying the linear power by $4.185 \cdot 10^{12}$ (neutrons/(cm^{2}s)/(kW/m)).

Table C.1. Main geometrical parameters.

Quantity	***Value***
Outer cladding radius (mm)	5.36
Inner cladding radius (mm)	4.74
Fuel radius (mm)	4.65
Fuel stack height (mm)	3055.0
Plenum height (mm)	127.0
Net plenum volume (mm^3)	18557

Table C.2. Main model selection of the TRANSURANUS input files.

Variable	**Value**	**Meaning**
IKUEHL	0	The coolant temperature is computed
IALPHA	0	Convective heat exchange coefficient of the coolant is calculated
IZENKA	0	Central void formation not considered
ISTZNE	0	Restructuring not considered
IPURE	0	Pu redistribution not considered
IOXIRE	0	Oxygen redistribution not considered
INTAXL	1	Interaction between fuel and cladding is considered
IHBS	1	High burn-up structure is considered only for thermal analyses
IRELOC	8	Modified FRAPCON-3 relocation model
IDENSI	2	Simplified densification model
IDIFSOLV	0	Intra-granular FGR computed by means of URGAS algorithm
FGRMOD	6	Matzke thermal coefficient, constant athermal coefficient
IGRBDM	1	Simple intergranular FGR. model (saturation concentration = constant)
MODFUEL(1:20)*	31	Standard LWR MOX fuel properties**
MODFUEL (4)	18	Fuel swelling modified FRAPCON-3 model
MODCLAD(1:20)	20	Standard LWR cladding properties
RRRR1	85000 (MWd/tHM)	Threshold BU from the HBS
KORNGR	0.073 (mm)	Fuel grain diameter
IFORM	5	Local power density calculated according to the TUBRNP model
OZUM0	2	Ratio between Oxygen and Metal (O/M)
PRODIS**	0.003975	Fraction of dish volume
POR000**	0.04375	Total fabrication porosity
DENPOR**	0.03038	Porosity at the end of sintering
DENBUP	3000 (MWd/kgHM)	Burn-up at which sintering has stopped
ISLICE	1	Slice option for the axial discretisation
M3	32	Number of slices
IWERT (9)	283 (°C)	Inlet coolant temperature
Pi0ein	2 (MPa)	Fill gas pressure at 25°C

* Except modfuel 4

** Standard LWR MOX fuel properties are the same as the standard LWR properties (MODFUEL(1:20) = 20), except for the thermal conductivity (MODFUEL(6))

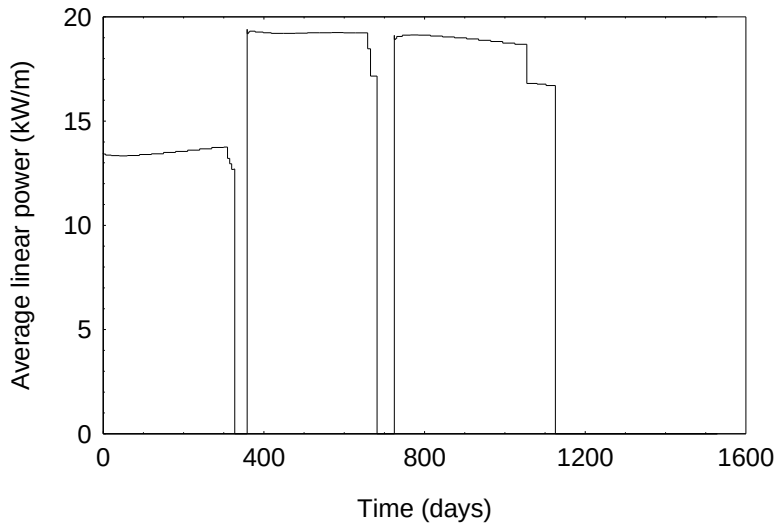

Figure C.1 Average linear power of one of the fuel rods of the assembly M501as a function of time. Two additional cycles of 17 kW/m have been added to reach a burn-up of about 50 MWd/kgHM.

(This page has been intentionally left blank)